

DTIC FILE COPY

1



National
Defence

Défense
nationale



AD-A220 817

SPECTRAL CHARACTERISTICS OF LOW-ANGLE RADAR GROUND CLUTTER (U)

by

H.C. Chan

DTIC
ELECTE
APR 24 1990
S B D

DISTRIBUTION STATEMENT A

Approved for public release
Distribution Unlimited

DEFENCE RESEARCH ESTABLISHMENT OTTAWA
REPORT NO. 1020

Canada

90 04 24

004

December 1989
Ottawa

~~90 04 10 045~~



National
Defence

Défense
nationale

SPECTRAL CHARACTERISTICS OF LOW-ANGLE RADAR GROUND CLUTTER (U)

by

H.C. Chan
Surface Radar Section
Radar Division

DEFENCE RESEARCH ESTABLISHMENT OTTAWA
REPORT NO. 1020

PCN
041LC12

December 1989
Ottawa

SPECTRAL CHARACTERISTICS OF LOW-ANGLE RADAR GROUND CLUTTER

ABSTRACT

A detailed analysis of low-angle ground clutter spectral characteristics was carried out using the MIT Lincoln Laboratory Phase I data and the DREO S-band clutter data. Both the fast Fourier transform and a super-resolution spectral analysis technique were used. Results showed that a ground-clutter spectrum comprises three components, namely, (a) a coherent component, (b) a slow-diffuse component and (c) a fast-diffuse component. Both the coherent component and the slow-diffuse component may be modelled as a symmetrical negative exponential density function. The fast-diffuse component may be modelled as a band-limited noise. Model parameters included the spectral slopes, the spectral density at zero-Doppler, and the cutoff frequency of the fast-diffuse component. The spectral slopes of the slow-diffuse component at various wind speeds have been calculated from the clutter data. The spectral densities of the various components were inter-related through wind speed and land cover. These parameters can be determined statistically from the clutter coherence factor for various land covers and wind speeds. The results of this analysis provided additional insights into ground clutter and can be used to develop signal processing techniques for improved low-velocity target detection in ground-clutter limited environment.

Accession For	
NTIS GRA&I	<input checked="" type="checkbox"/>
DTIC TAB	<input type="checkbox"/>
Unannounced	<input type="checkbox"/>
Justification	
By	
Distribution/	
Availability Codes	
Dist	Avail and/or Special
A-1	

Résumé

Nous présentons une analyse détaillée des caractéristiques spectrales du fouillis de sol vu à basse altitude. Les données utilisées proviennent du "MIT Lincoln Laboratory" et du CRDO, qui a recueilli ces données dans la bande S. Nous employons une technique super-résolutive et la transformée de Fourier rapide. Les résultats montrent que le spectre comprend trois parties, c'est-à-dire: a) une composante cohérente, b) une composante diffuse-lente et c) une composante diffuse-rapide. La composante cohérente et la composante diffuse-lente peuvent être représentées par une densité exponentielle. La composante diffuse-rapide peut être représentée par un bruit à bande étroite. Les paramètres du modèle indiquent les pentes du spectre, la densité spectrale à la fréquence Doppler nulle et la fréquence de coupure de la composante diffuse-rapide. Nous calculons aussi les pentes du spectre pour la composante diffuse-lente versus différentes vitesses du vent.

Les densités spectrales des différentes composantes se relient lorsqu'on considère les facteurs tels la vitesse du vent et la végétation. Ces paramètres peuvent être déterminés statistiquement à partir du facteur de cohérence du fouillis pour différentes végétations et vitesses de vent. Les résultats de l'analyse améliorent notre connaissance du fouillis de sol et peuvent être utilisés pour développer des techniques de traitement du signal en vue d'améliorer la détection de cibles lentes dans un environnement avec fouillis de sol limité.

EXECUTIVE SUMMARY

The performance of ground-based radars is affected by the spectral characteristics of ground clutter. Most signal processing algorithms designed to enhance detection performance are Doppler-frequency-sensitive. Some examples are the moving target indicator filter, Doppler processor and coherent clutter map. The performance of these signal processors deteriorates as the spectral width of the observed clutter increases.

The spectral spread of the clutter process observed in a given radar resolution cell is a consequence of the motion of objects relative to the radar platform. This could be caused by targets of opportunity such as automobiles or birds moving in the resolution cell. However, in most instances, it is wind-induced. Vegetation and tree leaves move even in a light breeze. Heavy objects and semi-rigid structures such as hydro wires and large tree branches can have limited movement in moderate to strong winds. Thus the clutter spectrum will depend on the radar frequency and site environment parameters such as land-cover and wind velocity.

In this work, we carried out a comprehensive spectral analysis of low-angle ground clutter, using the MIT Lincoln Laboratory Phase I data and the DREO S-band clutter data. Both the fast Fourier transform and a super-resolution spectral analysis technique were used. Results showed that a ground-clutter spectrum comprises three components, namely, (a) a coherent component, (b) a slow-diffuse component and (c) a fast-diffuse component. Both the coherent component and the slow-diffuse component may be modelled as a density function that decreases symmetrically and exponentially on each side of the zero-Doppler frequency. The fast-diffuse component may be modelled as a band-limited noise. Model parameters included the spectral slopes, the spectral density at zero-Doppler and the cutoff frequency of the fast-diffuse component. The spectral slopes of the slow-diffuse component at various wind speeds had been calculated from the clutter data. The spectral density of the various components were inter-related through wind speed and land cover. These parameters can be determined statistically from the clutter coherence factor for various land covers and wind speeds. The results of this analysis have provided additional insights into ground clutter and can be used to develop signal-processing techniques for improved low-velocity target detection.

TABLE OF CONTENTS

1. Introduction.	1
2. Ground clutter data base and spectral analysis.	2
2.1 Ground clutter data for spectral analysis.	2
2.1.1 The MIT Lincoln Laboratory Phase I data base.	2
2.1.2 DREO S-band experimental phased array radar.	3
2.2 Maximum entropy spectral estimation (MESE).	4
2.2.1 Heuristic explanation of the MESE.	6
2.2.2 Practical considerations of the MESE.	8
2.3 Spectral components of radar ground clutter.	9
2.4 Spatial averaging of ground-clutter spectra.	14
3. Spectral analysis results.	18
3.1 Composite clutter spectra from different land cover areas.....	18
3.1.1 Agricultural land cover.	18
3.1.2 Deciduous forested land cover.	22
3.2 A composite spectral model for low-angle ground clutter.	22
3.3 Model parameters and their dependence on wind velocity and land cover.	28
3.3.1 Spectral slopes of the coherent and the slow-diffuse components.	28
(a) Spectral slope of the coherent component.	28
(b) Spectral slope of the slow-diffuse component.	28
(c) Effect of wind speed.	30
3.3.2 Clutter coherence factor.	32
3.3.3 The fast-diffuse component.	38
4. Conclusions.	38
4.1 Summary of results.	38
4.2 Signal processing improvements for ground-based surveillance Radars.	40
(a) Adaptive ground-clutter filter.	40
(b) Coherent clutter map.	41
(c) Predictive coherent-clutter map.	42
5. References.	42
6. Acknowledgement.	43

LIST OF FIGURES

Figure 1.	A map of the DREO radar site.	5
Figure 2.	Schematic diagram of an autoregressive (AR) system.	6
Figure 3.	Schematic diagram of a non-recursive filter.	7
Figure 4	Sectional clutter waveform and the corresponding spectrum of an X-band experiment performed in Beiseker, Alberta.	10
Figure 5.	Comparison of spectra of UHF clutter computed using the FFT and the MESE.	11
Figure 6	S-band ground-clutter spectrum observed in a particular resolution cell at the DREO site.	12
Figure 7.	Sectional clutter waveform and the corresponding spectrum of data referred to in Figure 6.	13
Figure 8.	Sectional clutter waveform and the corresponding spectra for a neighbouring resolution cell.	15
Figure 9.	Comparison of the MESE and the FFT spectra for L-band clutter from a typical resolution cell in the REPEAT sector of Peace River South II, Alberta, using short data records.	17
Figure 10.	Average ME spectra of X-band clutter for the REPEAT sector of Magrath, Alberta.	19
Figure 11.	Average ME spectra of S-band clutter for the REPEAT sector of Magrath, Alberta.	19
Figure 12.	Average ME-spectra of L-band clutter for the REPEAT sector of Magrath, Alberta.	20
Figure 13.	Average ME-spectra of UHF clutter for the REPEAT sector of Magrath, Alberta.	20
Figure 14.	I-channel X-band clutter waveform from a typical resolution cell in the REPEAT sector of Magrath, Alberta.	21
Figure 15.	Average ME-spectra of X-band clutter for the REPEAT sector of Peace River South II, Alberta.	23
Figure 16.	Average ME-spectra of S-band clutter for the REPEAT sector of Peace River South II, Alberta.	23
Figure 17.	Average ME-spectra of L-band clutter for the REPEAT sector of Peace River South, Alberta.	24

Figure 18. Average ME spectra of UHF-clutter for the REPEAT sector of Peace River South II, Alberta	24
Figure 19. Sectional clutter waveform and the corresponding spectra for a DREO S-band experiment.....	25
Figure 20. An S-band clutter spectrum showing the fast-diffuse component as a band-limited noise on each side of zero-Doppler.	26
Figure 21. S-band clutter spectra of a resolution cell with forested land cover and a resolution cell with agricultural land cover at the DREO site.	26
Figure 22. Symbolic diagram of the composite ground-clutter spectral model.	28
Figure 23. Slope parameter of the slow-diffuse clutter component as a function of recorded wind speed.	29
Figure 24. ME spectrum of a UHF experiment at Peace River South II.	30
Figure 25. Comparison of typical clutter spectra of resolution cells in (i) upwind and (ii) cross-wind conditions.	31
Figure 26. Comparison of the distributions of the coherence factor for S-band clutter at the DREO site in different wind-speed conditions.	33
Figure 27. Distributions of the coherence factor for clutter in the REPEAT sector of Magrath, Alberta.	36
Figure 28. Distributions of the coherence factor for clutter in the REPEAT sector of Peace River South II, Alberta.	37

1. Introduction.

The performance of ground-based radars is affected by the spectral characteristics of ground clutter. Most signal processing algorithms designed to enhance detection performance are Doppler-frequency-sensitive. Some examples are the moving target indicator (MTI) filter [1], Doppler processor [2], and coherent clutter map [3]. The performance of these signal processors for low-Doppler targets deteriorates as the spectral width of the observed clutter increases.

Spectral behaviour of ground clutter has received less attention from radar researchers compared with other characteristics such as temporal and spatial amplitude statistics. Traditionally, clutter problems are treated by employing filters or cancellers. These filters usually have fixed band-pass characteristics. Targets whose Doppler is close to that of the clutter are also attenuated, thereby reducing their detection probability and resulting in the so-called blind-speed regions.

In the analysis of ground clutter it is sometimes convenient to assume that its spectrum has a simple analytical form such as a Gaussian spectral-density function. One can characterize a Gaussian ground-clutter spectrum centred about zero-Doppler by a single parameter, the 3 dB spectral width. Detailed analysis of data collected from ground-based radars revealed that the ground clutter spectrum is highly composite. There are several spectral components which have significantly more power than the receiver noise. Signal processing techniques developed based on only one spectral component may not perform as expected if other spectral components with significant power are not taken into consideration. It is therefore essential that we identify the various spectral components of clutter and evaluate their relative significance in terms of signal processing.

The spectral spread of the clutter process observed in a given radar resolution cell is a consequence of the motion of objects relative to the radar platform. This could be caused by targets of opportunity such as automobiles or birds moving in the resolution cell. However, in most instances, it is wind-induced. Vegetation and tree leaves move even in a light breeze. Heavy objects and semi-rigid structures such as hydro wires and large tree branches can have limited movement in moderate to strong winds. Thus the clutter spectrum will depend on the radar frequency and site environment parameters such as land cover and wind velocity.

This report presents the spectral analysis of ground clutter for different bands of radar frequency. In Section 2 we describe the data used in the spectral analysis. We employed both the conventional Fourier analysis and a super-resolution spectral analysis technique. Because of the relatively short observation time employed in some of the data, we found that super-resolution spectral estimation techniques were more suited for their analysis than the fast Fourier transform (FFT) method. A brief background on the maximum entropy spectral estimate (MESE) is given, and the particular procedure designed to bring out the spectral characteristics of ground clutter from short time series is described.

Section 3 presents the spectral analysis results. We summarize the observed ground-clutter spectral characteristics and correlate them with radar and site environment parameters. In section 4, we present conclusions on the spectral characteristics of low-angle ground clutter and outline signal-processing schemes for improving low radial-velocity target detection.

2. Ground-clutter data base and spectral analysis.

2.1 Ground-clutter data for spectral analysis.

Our data for spectral analysis came from two sources. The first was the MIT Lincoln Laboratory's Phase I ground-clutter data base [4]. The second was the Defence Research Establishment Ottawa (DREO) S-band phased-array radar.

2.1.1 The MIT Lincoln Laboratory Phase I Data Base.

The MIT Lincoln Laboratory Phase I [5] was an extensive program of ground-clutter data collection, analysis and modelling. The equipment employed included a mobile coherent radar, a multi-frequency antenna assembly, a versatile data-acquisition system and a fleet of tractor-trailers for transporting the facility. The essential characteristics of the Phase I facility is summarized in Table I.

Table I: Technical characteristics of the MIT Lincoln Laboratory Phase I radar facility

Frequency	165 MHz	430 MHz	1250 MHz	3400 MHz	9100 MHz
Antenna					
Azimuthal	13°	5°	3°	1°	1°
Beamwidth					
Waveform	High Resolution: 36 m		High Resolution: 15 m		
Resolution	Low Resolution: 150 m		Low Resolution: 150 m		
Polarization	Vertical Transmit/ Vertical Receive Horizontal Transmit/ Horizontal Receive				
PRF	500 to 4000 Hz				

Using the Phase I radar facility, Lincoln Laboratory personnel collected and calibrated ground clutter data from many U.S. and Canadian sites for all combinations of frequency bands, polarization and waveform resolution. These data were collected primarily in three modes: (i) SURVEY mode, (ii) REPEAT mode and (iii) HOP mode.

The SURVEY data were recorded with the antenna scanning at a maximum velocity of 3°/sec. With a scanning antenna, the successive returns of a transmitted pulse train are slightly displaced in azimuth. Consider an azimuthal sector the size of the antenna azimuthal beamwidth. The number of pulses which can be transmitted during the time the antenna moves from one side of the azimuthal sector to the other is called "hits per 3 dB beamwidth", defined as:

$$\text{Hits per 3 dB beamwidth} = \frac{\theta \times \text{PRF}}{\omega_s} \quad (1)$$

where θ is the antenna 3 dB beamwidth in degrees,
 PRF is the pulse repetition frequency in Hz, and
 ω_s is the antenna scanning velocity in degrees/sec.

The time required for a radar to transmit the number of hits per 3 dB beamwidth may be considered as the effective observation time of the returns coming from the centre of this azimuthal sector. For the Phase I SURVEY data, this effective length was relatively short. For example, with a 3 dB beamwidth of 1° and a scanning velocity of $3^\circ/\text{sec}$, it takes 0.333 seconds for the antenna to traverse one azimuthal beamwidth. For conventional Fourier analysis, the resolution of the spectrum is inversely proportional to the length of the observation interval. This means that the attainable resolution of conventional spectral estimation techniques for this data set is 3 Hz. Since the spectral content of most ground clutter extends only to several Hz (it could extend to several tens of Hz at X-band and at high wind speeds), a spectral resolution of 3 Hz cannot characterize most ground clutter spectra adequately. Thus the SURVEY data were not suitable to be used for spectral analysis.

The HOP data were the most suitable form of Phase I data for spectral analysis. The HOP data were recorded with a stationary antenna. Hence there was no antenna scanning modulation. The dwell time for the HOP data was usually quite long, from 20 seconds to about a minute. The PRF was 500 Hz. Thus it was possible to obtain spectral resolution as low as a fraction of a Hz. Unfortunately, there were not sufficient HOP data from each site with adequate range of wind speed to provide the necessary information on clutter spectral characteristics for modelling. The only exception was the Katahdin Hill, MA site where very detailed ground truth and a large amount of HOP data were collected. The analysis of these data has been reported by Billingsley and Larrabee [6].

This leaves the REPEAT data. The REPEAT data were collected over an azimuthal sector of 10 to 20 degrees in each site at different times. It permitted the observation of clutter from the same set of resolution cells at different winds speed and directions. The REPEAT data also employed a stationary antenna; however, the PRF was usually higher than that employed in the HOP experiments, typically from 2 to 3 kHz. The dwell was 1024 pulses, and for a PRF of 3 kHz, represented an observation period of only 341 msec. The FFT yielded poor results when it was used to analyze these data.

In Section 2.3 we will outline a procedure using the MESE to extract spectral information from the Phase I REPEAT data.

2.1.2 DREO S-band Experimental Phased Array Radar.

The DREO Radar Division's S-band coherent phased array radar facility provided suitable ground clutter data of the surrounding area for detailed spectral analysis. The advantage of this data source was that very long dwells could be used to obtain clutter data from individual resolution cells. For data collection, we employed a time series of

30720 pulses at a PRF of 100 Hz. This particular combination of PRF and number of pulses represents 307.2 seconds of observation time. The limitations of the DREO radar were that it was a single-band radar and that it transmitted and received only in horizontal polarization. The characteristics of the DREO Radar Division S-band Phased Array Radar are summarized in Table II.

TABLE II: CHARACTERISTICS OF THE DREO RADAR DIVISION
S-BAND PHASED ARRAY RADAR

FREQUENCY	2970 MHz
POLARIZATION	HORIZONTAL
PULSE WIDTH	1.0 μ s
PRF	100 Hz
PEAK POWER	2.5 KW
AZIMUTHAL BEAMWIDTH	4°

Figure 1 shows a map of the DREO site. The S-band phased array antenna can be electronically steered to cover an arc of 80°. We divided this arc into 20 look directions, each representing a 4° sector. The range extent for data collection was limited to about 10 km. Ground clutter data were taken directly from the In-phase (I) and Quadrature (Q) channels analog-to-digital converters(ADC). With a 150m (1 μ s pulse) range resolution, there were 1200 resolution cells. Excluding those located on the Ottawa River, data from approximately 600 resolution cells could be studied in detail. Three complete sets of clutter data were collected at winds speeds of 3, 12, and 25 mph respectively.

2.2. Maximum-entropy spectral estimation.

MESE is a family of algorithms which provides superior resolution capability for random data fitting the so-called autoregressive (AR) model. It is used extensively in the fields of acoustics and speech processing. Radar ground clutter, having low-frequency spectral characteristics, has attributes similar to those of an autoregressive random process. In Section 2.3 we shall give examples showing that ground clutter spectra can be approximated very well by AR models of moderate orders.

MESE assumes that a complex time series representing a sampled random process is the output of an autoregressive (AR) system driven by white noise. The AR system has the structure shown in Figure 2. Here the time series is taken from the output of an adder which sums the input noise sample with a number (M) of past output samples weighted by a set of complex coefficients $\{a_n\}$. The Z-transfer function of the system in Figure 2 is given by:

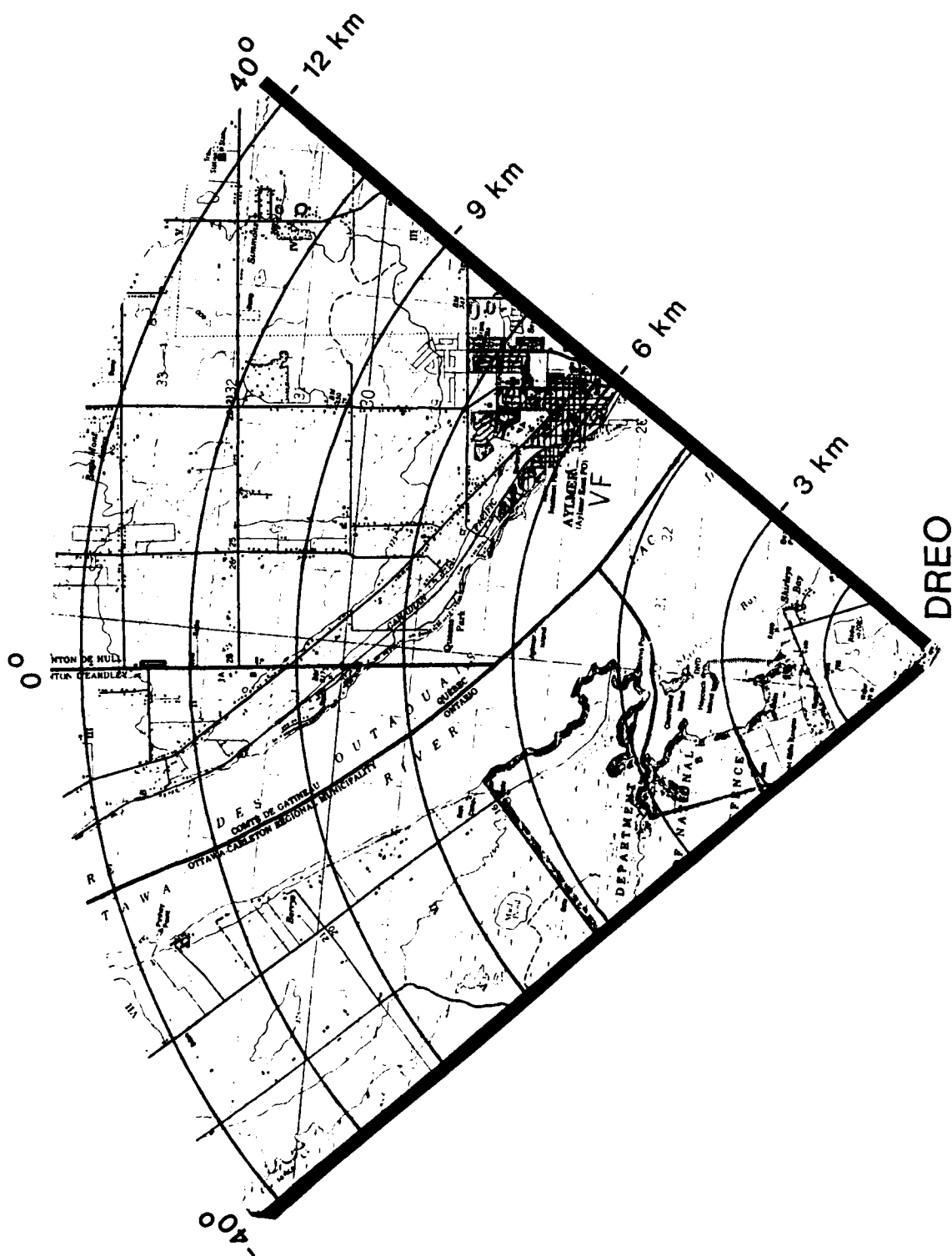


Figure 1. A map of the DREO radar site.

$$G(z) = \frac{1}{1 + \sum_{n=1}^M a_n z^{-n}} \quad (2)$$

where a_n , $n=1,2,\dots,M$ are complex numbers

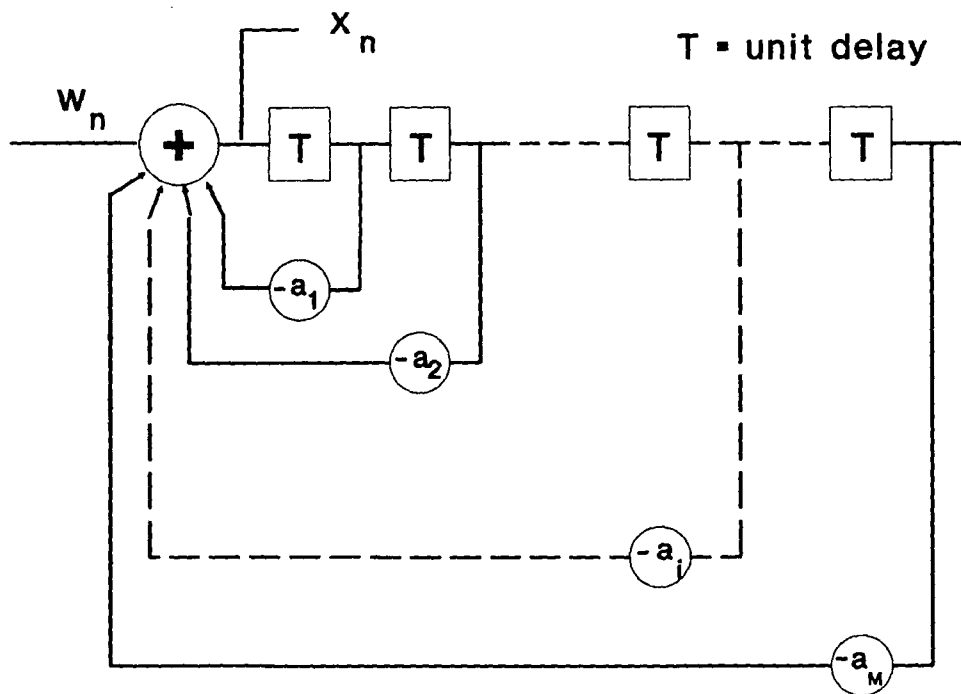


Figure 2. Schematic diagram of an autoregressive (AR) system.

2.2.1 Heuristic explanation of MESE

The concept of MESE can be explained using the following heuristic argument. If the input noise process is white (i.e., a flat input spectrum), the spectrum at the output of the AR system is proportional to its Z-transfer function. Consider a non-recursive filter whose structure is shown in Figure 3. The Z-transfer function of this filter is:

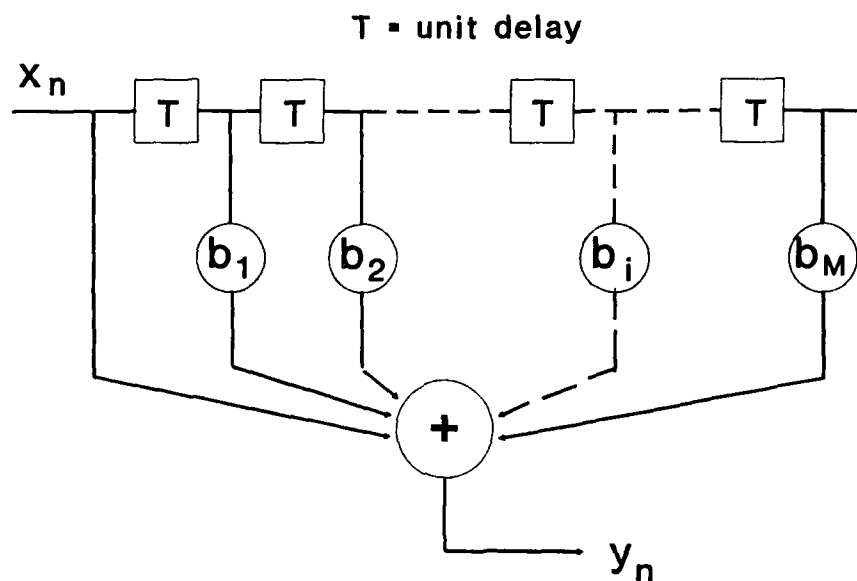


Figure 3. Schematic diagram of a non-recursive filter.

$$H(z) = 1 + \sum_{n=1}^M b_n z^{-n} \quad (3)$$

The denominator in Eqn(2) has the same form as that of the Z-transfer function of the recursive filter except for the coefficients. Suppose we cascade the AR system with this filter. The spectrum of the time series observed at the output of the non-recursive filter will be flat if $b_i = -a_i$, $i=1,2,\dots,M$, because in this case the denominator of the AR Z-transfer function cancels the Z-transfer function of the recursive filter, leaving a constant as the cascaded Z-transfer function.

The filter in Eqn(3) used in this context is a linear prediction filter [7]. The output of this filter represents the prediction error. The greater the mismatch between $\{a_i\}$ and $\{b_i\}$, the greater the prediction error would be. The prediction error power is a function of the covariance matrix of the time series and the coefficients $\{a_i\}$. Since the input spectrum is flat, to calculate an AR spectrum, it suffices to find the set of coefficients $\{a_i\}$ that minimizes the prediction error power. The detailed development of the MESE is well documented [7-9].

There are many variations in the realization of the MESE. We adopted a particular algorithm due to Burg[8] in our analysis. After finding the AR coefficients $\{a_i\}$ and the prediction error power P_{M+1} , the clutter spectrum is given by:

$$S(f) = \frac{P_{M+1} \Delta t}{\left| 1 + \sum_{n=1}^M a_n \exp(-j2\pi n f \Delta t) \right|^2} \quad (4)$$

where f is the Doppler frequency, and Δt is the sampling interval of the time series.

In Eqn(4) the Doppler frequency f is a continuous variable. In practice, the ME-spectrum is computed at regular discrete points within the Doppler band. With the Doppler bandwidth normalized to unity, Eqn(4) was evaluated at regular intervals of $f=k\Delta f$, $k=0,1,2,\dots,K$, where $\Delta f=1/K$. To obtain good spectral resolution, we chose a value of $K=1024$ points. Thus each discrete value computed from Eqn (4) represents the clutter power in the region : $k\Delta f < f < (k+1)\Delta f$.

2.2.2 Practical considerations of the MESE

In applying the MESE, there are two parameters to be considered. The first is the order (M) of the AR process to be postulated. The MESE essentially approximates the clutter spectrum by allocating the poles of the AR process in such a way that the resulting Z-transfer function of the AR process is very similar to the clutter spectrum. This is analogous to the synthesis of a band-pass characteristic by means of a bank of tuned filters. The ability of the filter bank to approximate a given transfer function is dependent on the number of filters in the filter bank and the complexity of the transfer function. The more complicated the transfer function the greater the number of filters that is required. The appropriate order of an AR model fitting a given time series may be determined from consideration of Akaike's final prediction error [10] for an N -point time series. For long time series (>1024 samples) we used an order $M = 50$. For short time series (< 32 samples), we limited the order of the AR model to a quarter of the length of the time series. Both cases yielded good spectral estimates.

The second parameter is the signal bandwidth of the clutter. The unambiguous bandwidth over which the clutter spectrum can be measured is determined by the PRF. The PRF employed in the Phase I REPEAT data was either 2 kHz or 3 kHz. Examination of ground clutter at various frequencies and wind conditions indicated that the spectral spread of ground clutter ranges from within ± 1 Hz at VHF to ± 50 Hz at X-band. At S-band, where the DREO radar operates, the spectral extent (the Doppler region in which the clutter spectral density is greater than the receiver noise density) of clutter is less than ± 25 Hz even in fairly strong winds.

If the PRF is much greater than the spectral extent of the clutter, some of the poles of the AR model will be located in the portion of the spectrum that is occupied essentially by receiver noise. As a result, only a small fraction of the poles would be allocated to the clutter spectrum. To obtain a good approximation of the clutter spectrum, a larger value of M is required than would be for a smaller PRF.

One way to reduce the order of the AR model and still retain the accuracy of the clutter spectral estimate is to coherently integrate the time series before performing MESE. The integration may be more appropriately described as coherent block-averaging. That is, a block of K contiguous samples of the original time series is coherently summed and the result divided by K . However, for simplicity, we will use the term "coherent integration" to describe the above operation. A coherent integration of a time series over K samples is equivalent to low-pass filtering the data with a filter having $1/K$ the original bandwidth. As long as the resulting bandwidth is still much greater than the clutter spectral spread, negligible information loss on the clutter will result.

There is a drawback in applying coherent integration before performing spectral analysis. Strong spectral components of targets of opportunity such as automobiles could fold back onto the reduced Doppler band because of the aliasing effect. Fortunately, these components appear as narrow spectral lines and can be readily distinguished from that of ground clutter.

2.3 Spectral components of radar ground clutter

To gain some insight into the origin of the spectral components in a clutter process, we examined the clutter spectrum together with the clutter waveform. The spectral plots are given in terms of relative magnitudes in dB with respect to a numerical value of unity. For the purpose of analyzing spectral characteristics, the absolute magnitude of the clutter is not important.

Figure 4 shows the in-phase channel waveform together with the corresponding spectrum of an experiment performed in Beiseker, Alberta. The experimental parameters were: X-band, horizontal polarization, 150 m waveform resolution, Azimuth = 314.7° , Range = 1266 m, PRF = 1.0 kHz, observation interval = 20.48 seconds (20480 pulses). The entire waveform was divided into blocks of 1024 samples. For each block, we calculated the spectrum using the FFT and a Blackman window and plotted them in alternate rows of figures. The horizontal axis in each spectrum-block represents a range of Doppler frequency from -500 Hz to 500 Hz.

We can see how the clutter spectrum behaved in contiguous time frames of one second by examining the spectra of successive waveform segments. A narrow spectral line and a low-frequency spectral component centred about zero-Doppler were always present. There were also the receiver noise component and a few periodic spectral lines, probably caused by the harmonics of the 60 Hz power supply. The rapid modulation waveform of frames two to five (pulse number 1024 to 5120) appeared as a Doppler shifted spectral component. The Doppler shift was seen to have increased to over 600 Hz. A Doppler shift of 600 Hz corresponds to a velocity of 22 mph at X-band. This was faster than the recorded wind speed of 13 mph. The high velocity and the fact that the acceleration was in one direction indicated that the object in motion was free, perhaps a flock of birds.

A less rapid modulation waveform appeared from frame No.9 to No.14. This modulated waveform can be identified from the corresponding spectrum of the waveform segments as a slightly Doppler-shifted spectral component around zero. The origin of this component is less obvious. In all probability, it was caused by a combination of slow-flying birds and a sudden wind gust which accelerated objects such as tree leaves and branches.

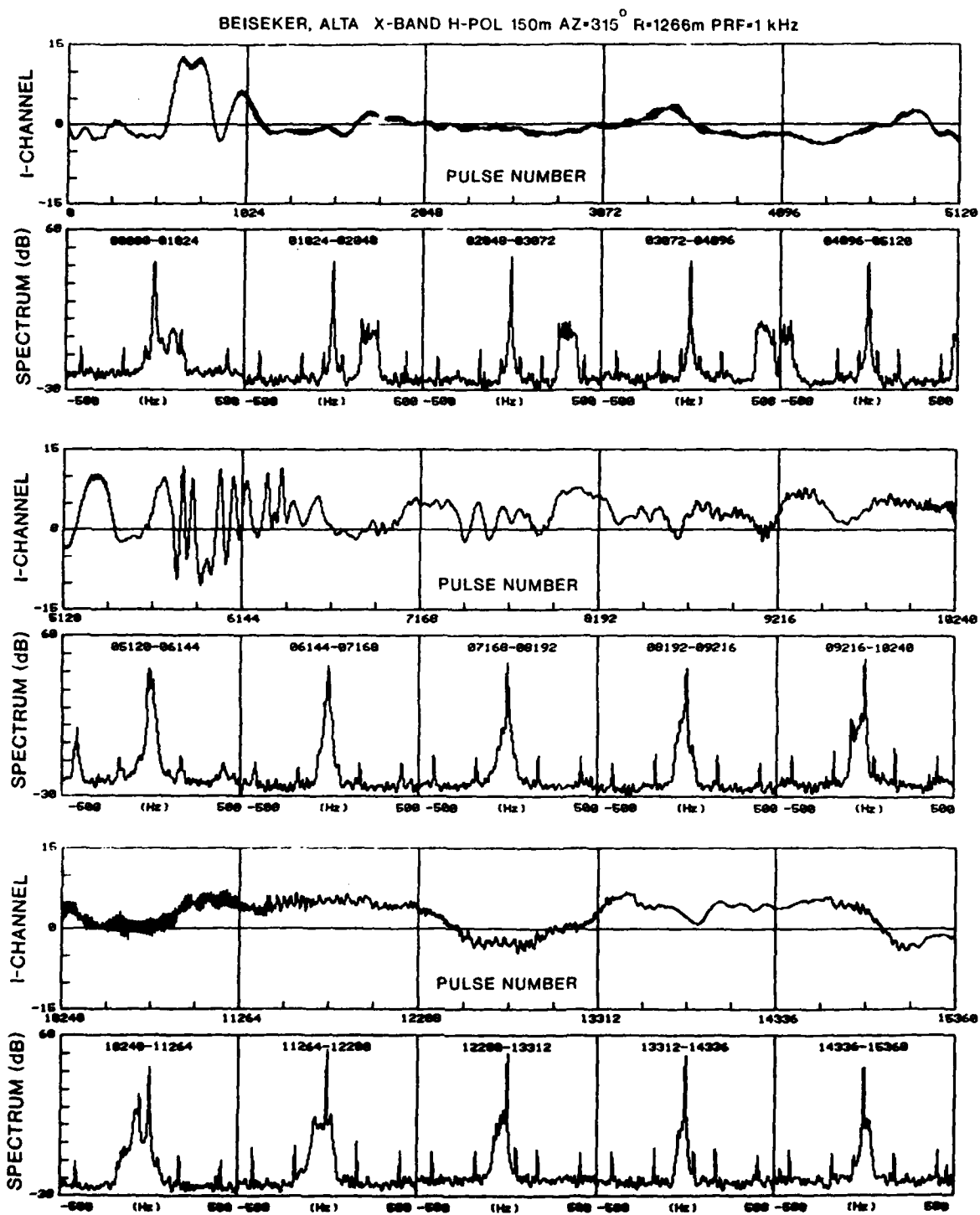


Figure 4 Sectional clutter waveform and the corresponding spectrum of an X-band experiment performed in Beiseker, Alberta.

Analysis of available HOP data at other frequencies showed similar results, except for UHF at low wind speeds. At UHF, the slow-diffuse component was often below noise level. Figure 5 compares the spectra of a UHF experiment computed using the FFT and the MESE. The experimental parameters are given in the Figure.

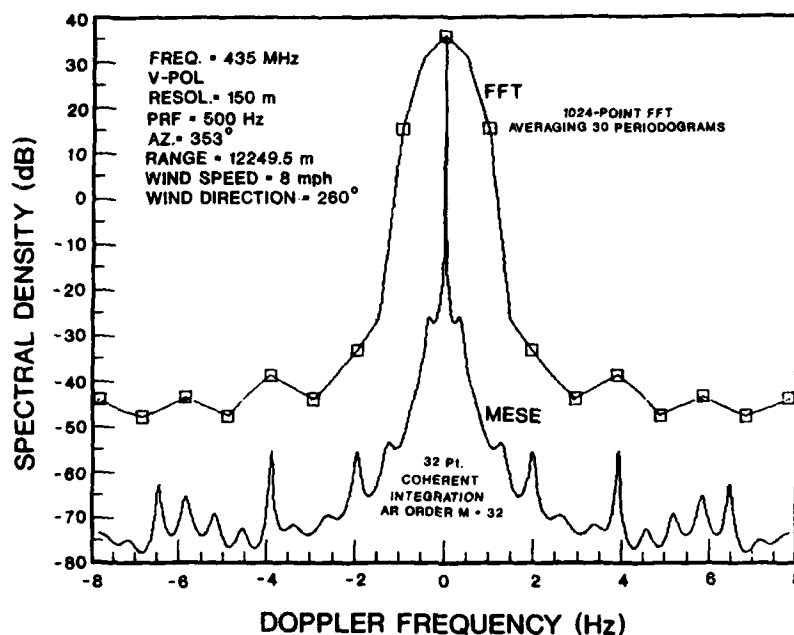


Figure 5 Comparison of spectra of UHF clutter computed using the FFT and the MESE.

The original 30720-point time-series was partitioned into thirty 1024-point subsequences. The FFT was performed on each subsequence using a Blackman window. The upper curve in Figure 5 was obtained by averaging the thirty periodograms. The spectral extent of the FFT spectrum was equal to the PRF (500 Hz). Hence there were only 32 samples in the Doppler region of ± 8 Hz. Only the coherent component was visible from the FFT spectrum, and it was masked by the data window. Improved spectral resolution can be obtained by performing a single 30720-point discrete Fourier transform; however, the resulting periodogram was very spiky, and the diffuse components were masked by the receiver noise. The lower curve was the ME-spectrum obtained using the following parameters: 32-point coherent integration, AR model order $M=32$. With the 32-point coherent integration, the noise floor was reduced, and the slow-diffuse component became visible.

Three spectral components may be identified as those of ground clutter, namely, (a) a coherent component, (b) a slow-diffuse component and (c) a fast-diffuse component. The coherent component occupies a very narrow spectral region around zero Doppler whose width was a function of the radar frequency, wind speed and land cover. The spectral width ranged from practically zero for VHF (or for urban land cover, i.e., buildings) up to several Hz for X-band.

The slow-diffuse component occupied a broader Doppler region than the coherent component. Again it was a function of the radar frequency and wind speed. The Doppler region of this component could extend to several tens of Hz at X-band. The magnitude of the slow-diffuse component relative to the coherent component decreases with decreasing radar frequency.

The fast-diffuse component occupies a even broader Doppler region than the slow-diffuse component. It was localized, ie., this component might be present in clutter from one resolution cell while it was absent in the clutter of the neighbouring resolution cells during the same observation interval.

In order to assess the relative significance of various spectral components of ground clutter, we used data collected from the DREO S-band radar. Figure 6 shows the averaged spectrum of the clutter obtained from a particular resolution cell in the DREO site. The experimental parameters are given on the figure.

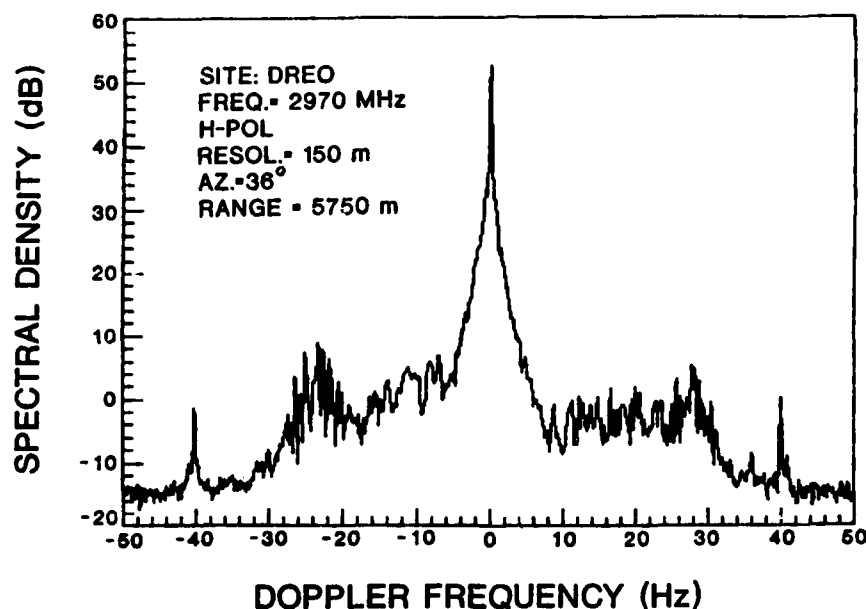


Figure 6. S-band ground clutter spectrum observed in a particular resolution cell at the DREO site.

In this clutter spectrum, the fast-diffuse component appeared as a band-limited noise in the averaged clutter spectrum (a more or less flat spectral density between ± 30 Hz). However, it actually comprised narrow-band components which appeared at different times. To see this, we plotted the I-channel waveform and the corresponding spectra of the clutter data of Figure 6 in Figure 7.

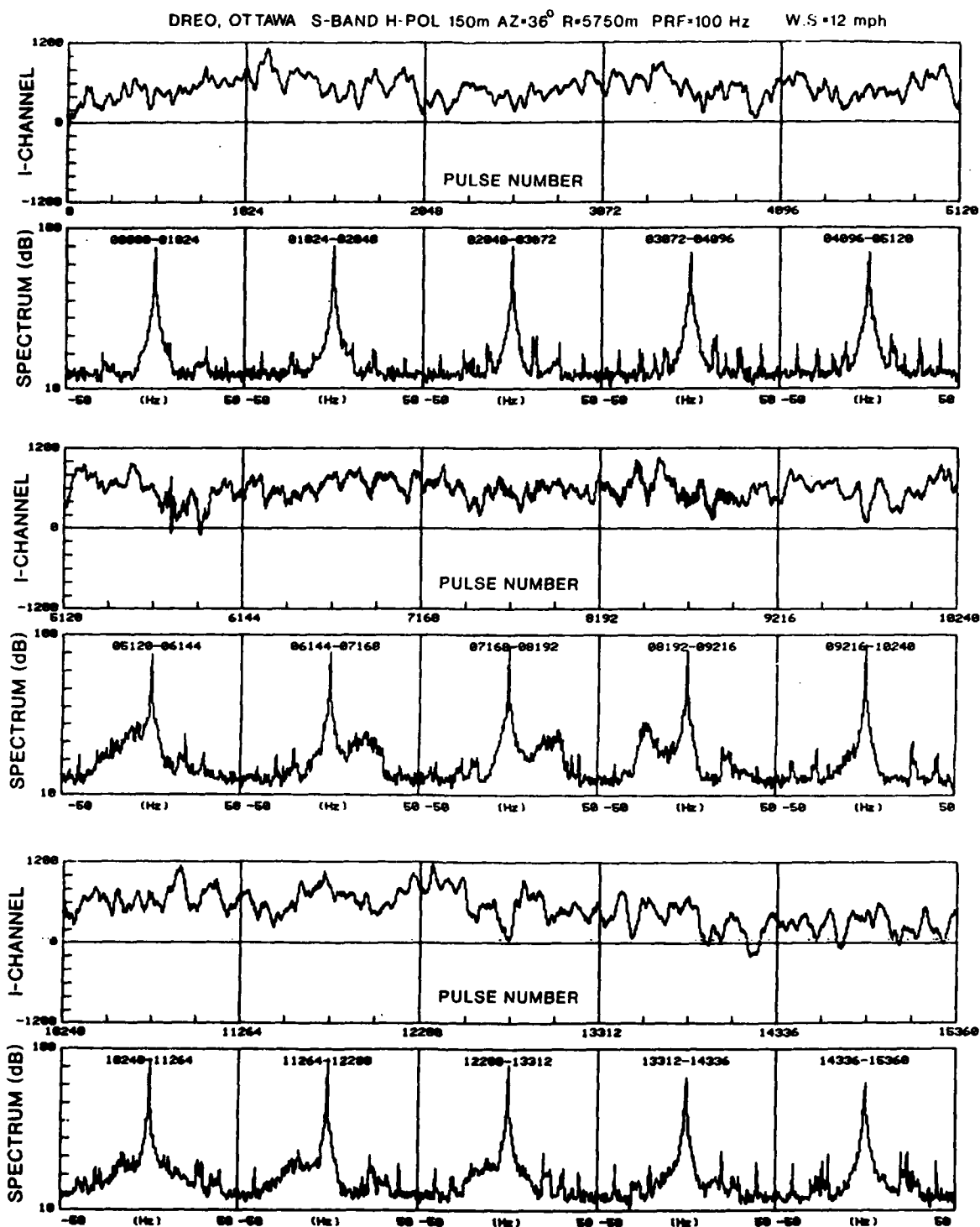


Figure 7. Sectional clutter waveform and the corresponding spectrum of data referred in Figure 6.

From Figure 7, we noticed a rapid modulation of the clutter waveform appearing from the middle of frame No. 6 to about frame No. 10 (pulses 5120 - 10240; approximately 40 seconds). The Doppler shift of this component varied with time as can be seen from the corresponding spectra. In Figure 8 we showed the I-channel waveform segments and the corresponding spectra for a resolution cell which was about 600 m beyond the one whose waveforms were shown in Figure 7. There was no noticeable fast-diffuse component in the spectra of Figure 8. Since the two waveforms were sampled simultaneously, this indicated that the fast-diffuse component was transient in nature and that its occurrence is the result of a localized wind gust.

For the resolution cell whose clutter spectrum was shown in Figure 6, aerial photographs showed that the cell was located at the far shore of the Ottawa River, and that there were a few isolated trees within the cell. Thus the coherent component resulted from the strong echo from the shore line, and the slow and diffuse components resulted from the motions of the trees. To get a first-order estimate of the relative significance of these three components, we integrated the spectral density of Figure 6 in three Doppler regions: (a) coherent component from -0.2 Hz to $+0.2$ Hz, (b) slow-diffuse component from -8 Hz to -0.2 Hz and 0.2 Hz to $+8$ Hz, and (c) fast-diffuse component from -35 Hz to -8 Hz and $+8$ Hz to $+35$ Hz. We normalized the power of the diffuse components with respect to the coherent component. The slow and fast-diffuse components were estimated to be -9.34 dB and -28.8 dB, respectively, below the coherent component. The receiver-noise component was estimated to be -41 dB. It should be emphasized, however, that the relative magnitude of these components was dependent on frequency, land cover and wind speed.

2.4 Spatial averaging of ground-clutter spectra

The Phase I data base was valuable in that it was multi-frequency, multi-resolution and dual-polarization. The limitation was that the observation period was relatively short. In Section 2.2 we introduced the MESE which is superior to the FFT for analyzing short time series. However, the maximum entropy (ME) spectra using a single short time series cannot be considered representative. An average of many clutter spectra estimated from independent short-time series is needed to provide a representative ground-clutter spectrum.

If the clutter processes from a number of range cells of an area with similar land-cover are available simultaneously, a representative clutter spectrum for the area may be obtained by averaging the clutter spectra of the individual resolution cells.

In Section 2.3 we observed that the ground-clutter spectrum comprised a coherent component, a slow-diffuse component and a fast-diffuse component. The coherent component was spatially inhomogeneous in that its magnitude could vary more than 20 dB among neighbouring resolution cells. This is because the main contributors to the coherent component are usually man-made objects such as buildings, hydro towers, grain silos or natural features such as the ground, mountains, terrain ridges, river banks and tree trunks. The location of these natural and man-made features is site-dependent, and the effective radar cross-section of these objects is deterministically unpredictable due to propagation effects. The fast-diffuse component was transient in nature and could also be spatially inhomogeneous. Over a small area of similar land covers, however, the slow-diffuse component was more homogeneous. Thus a good representation of the slow-diffuse component for a patch area can be obtained by averaging the clutter spectra of resolution cells inside the area.

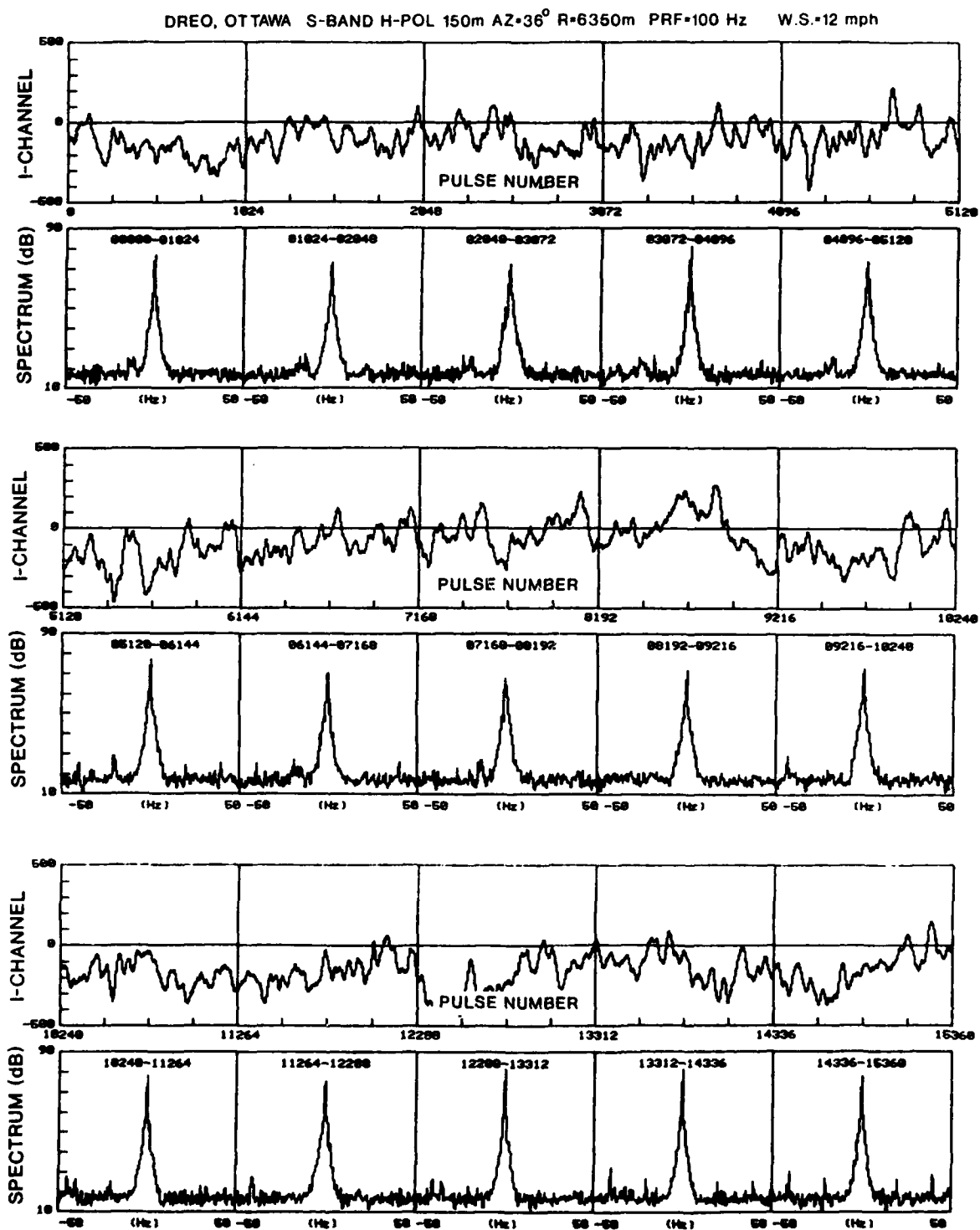


Figure 8. Sectional clutter waveform and the corresponding spectra for a neighbouring resolution cell.

Consider a small area which measures a few degrees in azimuth and approximately 1 km in range. For a range resolution of 150 m, this area may contain several tens of resolution cells. The PHASE I data have been calibrated to remove the (range)⁻⁴ dependence. However, the clutter magnitude is still directly proportional to range because the resolution cell size increases with range. Consequently the clutter spectra of individual resolution cells are normalized to that of the cell closest to the radar (r_1). We used the following procedure to obtain a representative ground clutter spectrum for such a patch area.

Let $S_{ij}(f)$, $i=1,2,\dots,I$; $j=1,2,\dots,J$ be the short-term (calculated using short time series records) clutter spectra of the resolution cell located at the i th azimuth and the j th range. The averaged clutter spectrum for this area is defined as:

$$S(f) = \frac{1}{IJ} \sum_{i=1}^I \sum_{j=1}^J \frac{r_1}{r_j} S_{ij}(f) \quad (5)$$

where

r_j = the distance of the j th range from the radar

The accuracy of the clutter spectrum obtained using the above procedure depends on the spectral width of the clutter process and the relative magnitude of the coherent and diffuse components. In practice, if the coherent component is substantially higher than the slow-diffuse component and the spectral width of the slow-diffuse component is small, then the ME-estimate of the diffuse component using short data records will be unreliable. The reason is that, in this case, the spectrum around zero-Doppler is dominated by the coherent component. Nevertheless, the MESE will still provide a better result than that obtained using the FFT for the same record length.

As an example, Figure 9 compares the MESE and the FFT spectra of the L-band clutter for a resolution cell in the REPEAT sector of the Peace River South II, Alberta site. The experimental parameters are given in the figure. The FFT spectrum was computed directly from a single 1024-point clutter time series using a Blackman window. The ME spectrum was obtained by first coherently integrating the 1024-point time series over 16 samples and using an AR model of order 16. The reduction of the noise floor of the ME spectrum was the result of the coherent integration. It can be seen that the ME spectrum preserved the very narrow spectral line of the coherent component while the FFT spectrum was dominated by the spectrum of the data window.

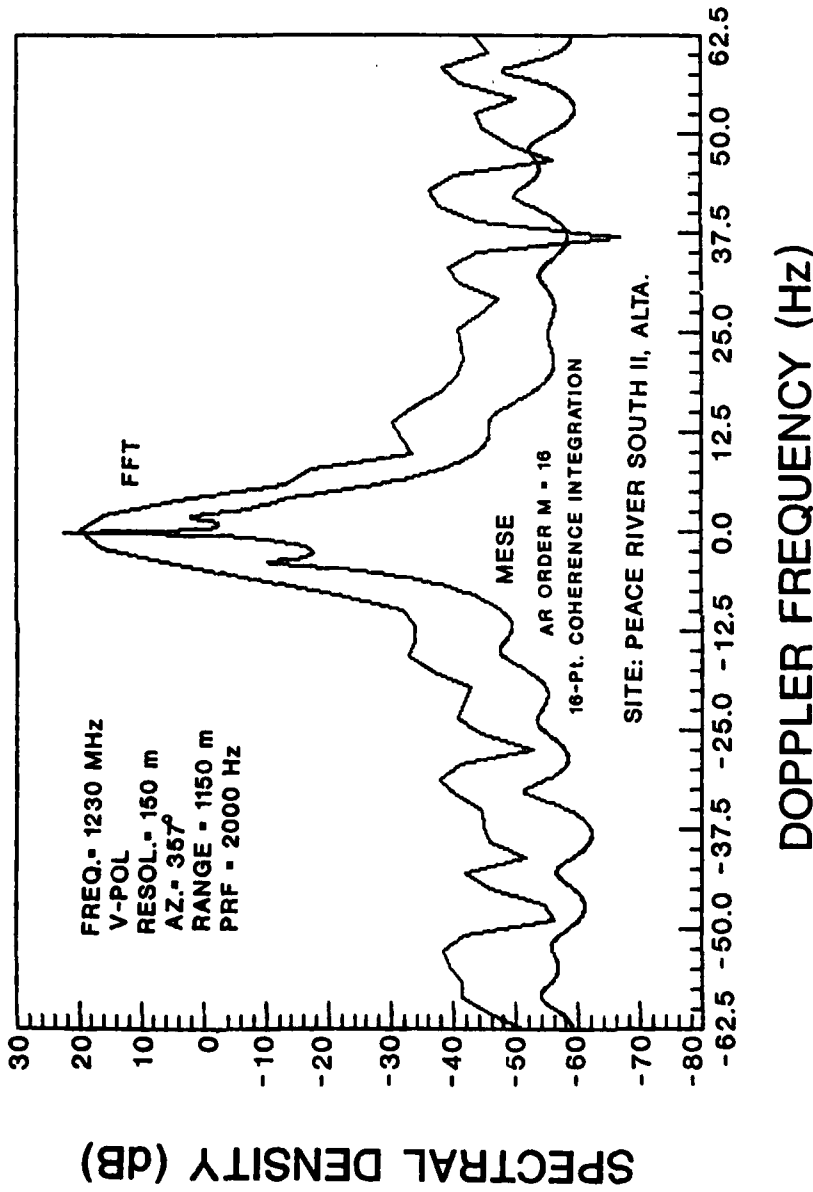


Figure 9. Comparison of the MESE and the FFT spectra for L-band clutter from a typical resolution cell in the REPEAT sector of Peace River South II, Alberta, using short data records.

3. Spectral analysis results.

3.1 Composite clutter spectra from different land cover areas

3.1.1 Agricultural land cover.

Figures 10 to 13 show the averaged ME spectra for clutter of the Magrath REPEAT sector at X-, S-, L- and U-bands, respectively. Vertical polarization data were used. The area in this sector had been classified to be principally agricultural lands. The spectra were calculated using the procedure outlined in Section 2.4. The wind speeds at the time the data were recorded for each spectrum are indicated in the figures. In general we noted the following:

(i) the rate of change (slope) of the power spectral density for the slow-diffuse component with Doppler frequency in dB scale was approximately linear, and

(ii) the slope decreases with increasing wind speed.

A linearly decreasing spectrum in dB scale suggested that the spectral density may be modelled by a function that decreases symmetrically and exponentially on each side of the zero-Doppler frequency. This relationship was reported by Billingsley and Larrabee [6] in their analysis of spectra from wind-blown trees. Our analysis of clutter in agricultural and urban areas indicated that the exponential model was also valid for clutter from crops and vegetation.

Figure 11 shows the averaged ME spectra for the same area at S-band, vertical polarization. The wind speeds for the three spectra were 2, 12 and 22 mph. We obtained results similar to those for X-band. The original PRF employed for these data was 3 kHz. In the spectral calculation, the data were first coherently integrated over 16 consecutive pulses, thereby reducing the bandwidth to ± 97.5 Hz. The spurious spectral lines were traced back to data from cells with automobile traffic. Assuming a nominal speed of automobiles of 30 mph or 13.4 m/sec, the corresponding Doppler shift is 268 Hz at S-band. The radar echo from automobiles is usually quite large. Thus spectral lines for an automobile travelling towards or away from the radar would appear as an aliased spectral line with reduced magnitude (after coherent integration). These spectral components were easy to identify because they were narrow in Doppler extent and they usually had a uni-directional Doppler shift. Similar results were observed for L-band and UHF data at relatively high wind speeds (>18 mph) as shown in Figures 12 and 13, respectively. It was not possible to obtain accurate spectral shape for the slow-diffuse component at VHF. The coherent component at VHF was observed to be several orders of magnitude higher than the diffuse components.

An interesting phenomenon was observed in an X-band, V-POL experiment at Magrath, Alberta (Figure 10). Apart from the usual large coherent component and a small diffuse component centred about zero Doppler, we observed two distinct spectral components centred about ± 27 Hz.

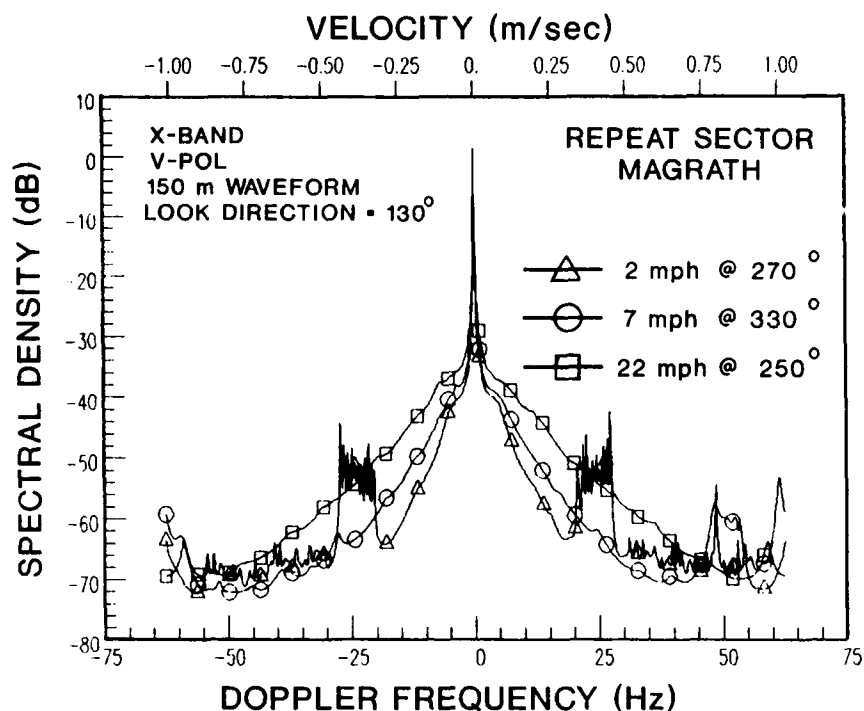


Figure 10. Average ME spectrum of X-band clutter for the REPEAT sector of Magrath, Alberta.

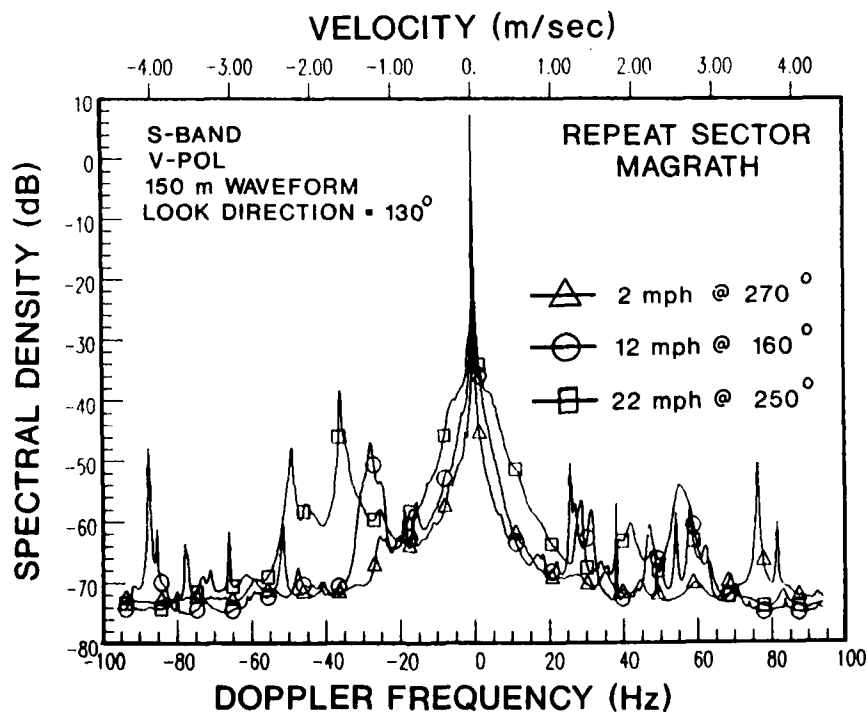


Figure 11. Average ME spectrum of S-band clutter for the REPEAT sector of Magrath, Alberta.

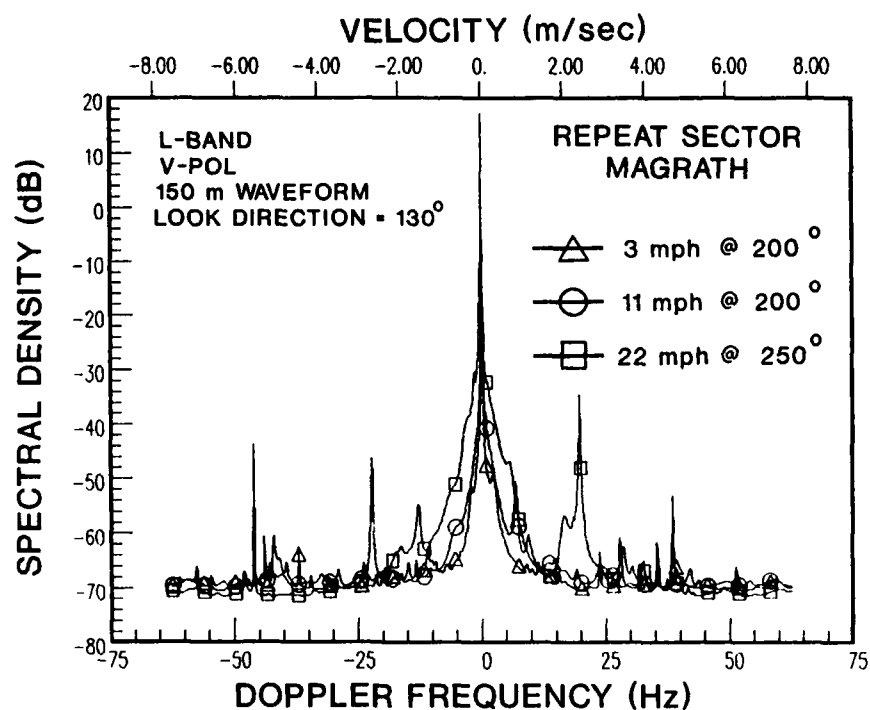


Figure 12. Average ME Spectrum of L-band clutter for the REPEAT sector of Magrath, Alberta.

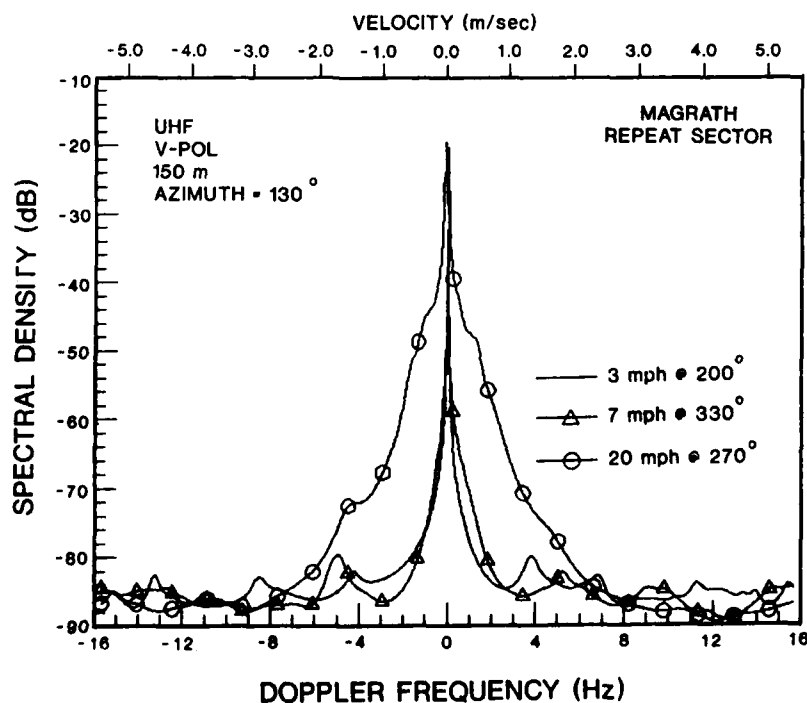


Figure 13. Average ME spectrum of UHF clutter for the REPEAT sector of Magrath, Alberta.

Careful examination of the coherent waveforms of the clutter data over the area revealed that this component existed in clutter data from most of the resolution cells. Figure 14 shows the I-channel waveform of the clutter data from one particular resolution cell which was typical of the entire area. The nominal period of the small sinusoidal component was estimated to be about 37 msec. This corresponded to a Doppler frequency of 26 Hz, as indicated in the spectrum.

A Doppler shift of 26 Hz at X-band corresponded to a velocity of 0.44 m/sec. The recorded wind speed of this experiment was 2 mph or 0.9 m/sec. This indicated that the spectral peaks centred about ± 27 Hz was probably the result of regular oscillatory motion of vegetation, arising from restricted freedom of travel and natural elasticity. If the wind speed is high, the motion of the crops is disrupted, forming what appears to be a band of random noise. This could explain the absence of these spectral components at higher wind speeds. It will be shown in Section 3.1.2 that this pendulum motion was also observed in some DREO S-band data taken in moderate wind conditions.

Clutter spectra were also analyzed for data taken using high resolution waveforms (15 m and 36 m). No significant difference was observed in the clutter spectral shapes between high- and low-resolution waveforms. Averaged clutter spectra computed from horizontal polarization data were similar.

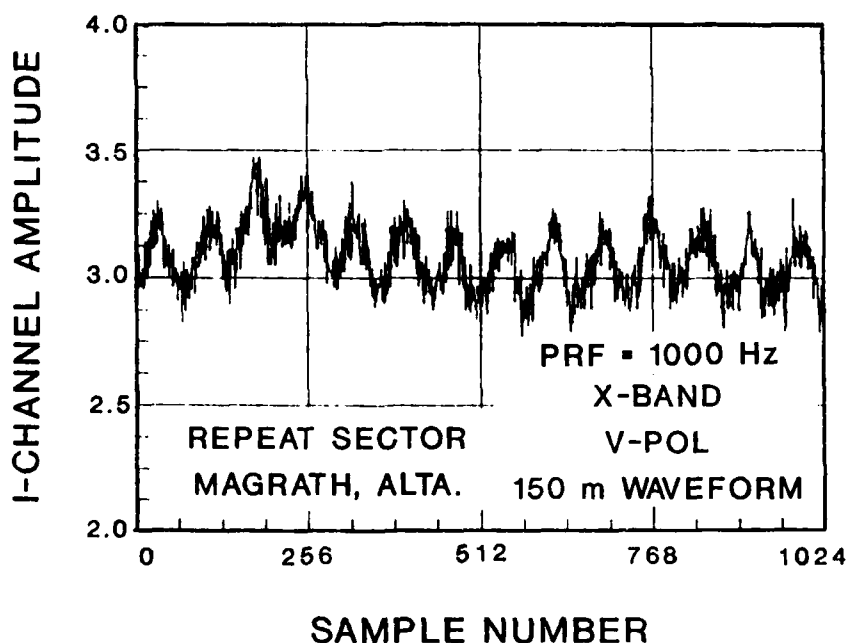


Figure 14. I-channel X-band clutter waveform from a typical resolution cell in the REPEAT sector of Magrath, Alberta.

3.1.2 Deciduous forested land cover.

Figures 15 to 18 show the averaged ME spectra for clutter processes in the REPEAT sector of Peace River South, Alberta for X-, S-, L-, and U-bands respectively. Land cover for this area was classified as deciduous forest. The clutter spectra were observed to comprise mainly the coherent component and a diffuse component. Again the diffuse-component power decreased exponentially with increasing Doppler frequency. The ratio between the coherent and diffuse components was generally smaller than that observed in the Magrath site. The dominant scatterers of forested terrains are trees. Since tree branches and leaves which have limited degree of freedom constitute a large proportion of a tree. The diffuse component of clutter from forested areas should be proportionately greater than it would be for urban and agricultural areas.

For S-band, we had a large amount of horizontal-polarization data from the DREO site. We used these data to examine the various spectral components in more detail. Figure 19 shows I-channel waveform together with its sectional spectra for a DREO S-band experiment. The recorded wind speed was about 12 mph. It can be seen that in successive 10-second time frames, two distinct fast-diffuse components on each side of the zero-Doppler were present. The Doppler shifts of the fast-diffuse component also appeared to vary with time, resulting in an averaged clutter spectrum with a band-limited noise on each side of the zero Doppler, as shown in Figure 20.

Comparing the results between agricultural and forested areas, we did not find significant difference in the slope of the clutter spectra for the same wind speed between the two land covers. This was supported by analysis of the DREO S-band data. We compared the clutter spectra of two groups of resolution cells. The first group represents cells with trees, and the other represents cells with crops only. The identification was based on high-resolution aerial photographs of the area. Figure 21 compares the clutter spectra of a representative cell from the forest group and one from the agricultural group, respectively. The recorded wind speed was 25 mph. As can be seen the slopes of the slow-diffuse component were very similar.

3.2 A composite spectral model for low-angle ground clutter.

Based on the above observations, we can postulate that the spectrum of ground clutter comprised three components:

$$S(f) = C(f) + D^s(f) + D^f(f) \quad (6)$$

where $C(f)$ is the coherent component; $D^s(f)$ and $D^f(f)$ are the slow- and fast-diffuse components, respectively.

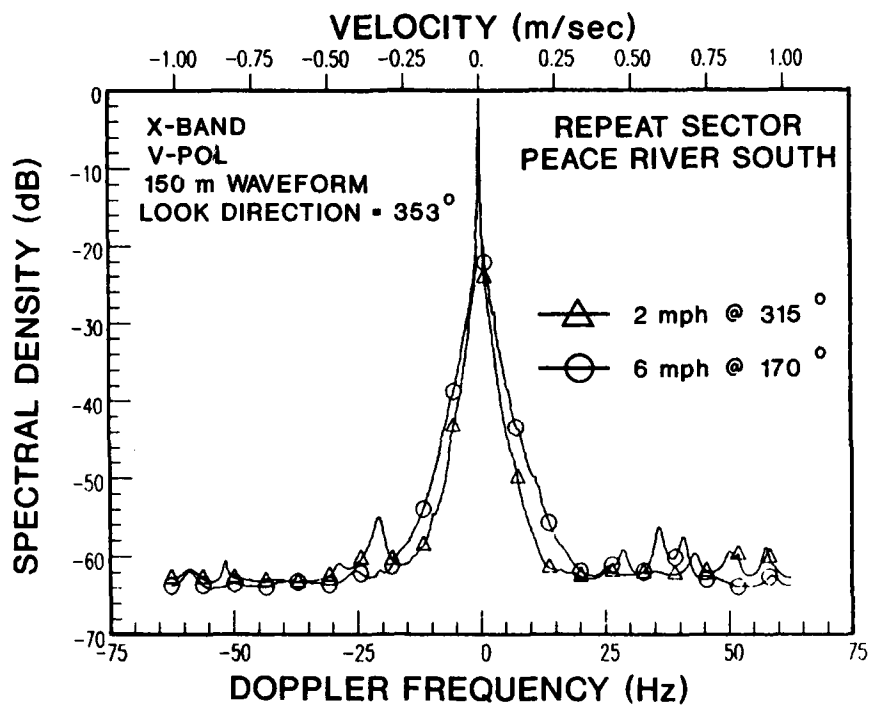


Figure 15. Average ME spectra of X-band clutter for the REPEAT sector of Peace River South II, Alberta.

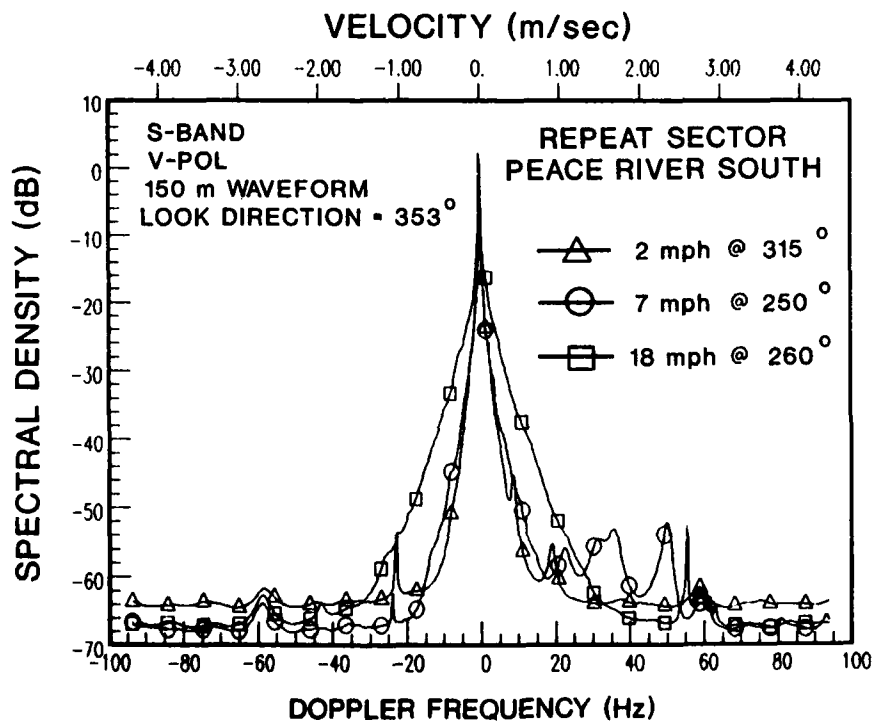


Figure 16. Average ME spectra of S-band clutter for the REPEAT sector of Peace River South II, Alberta.

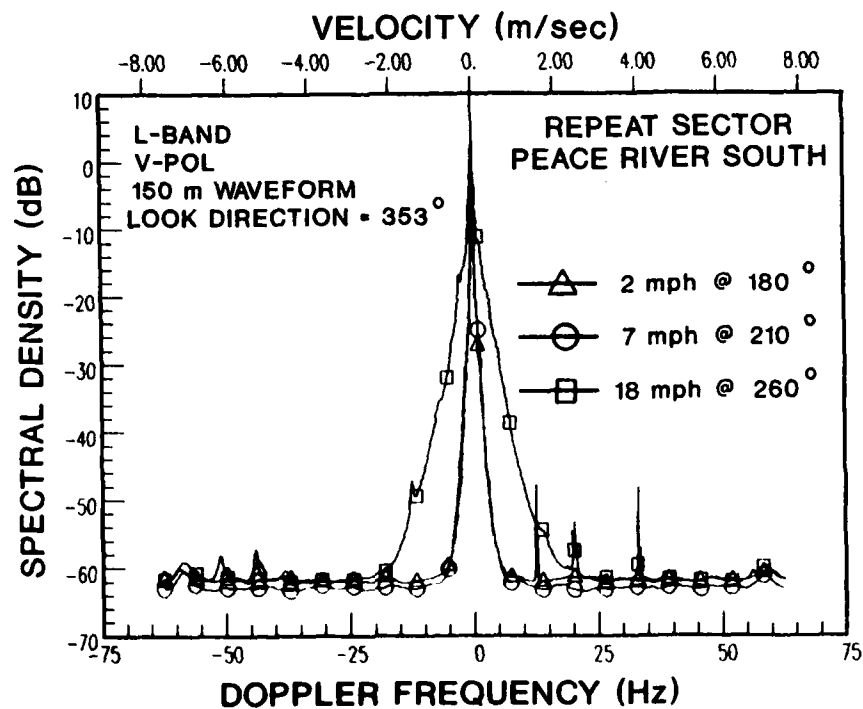


Figure 17. Average NE spectra of L-band clutter for the REPEAT sector of Peace River South II, Alberta.

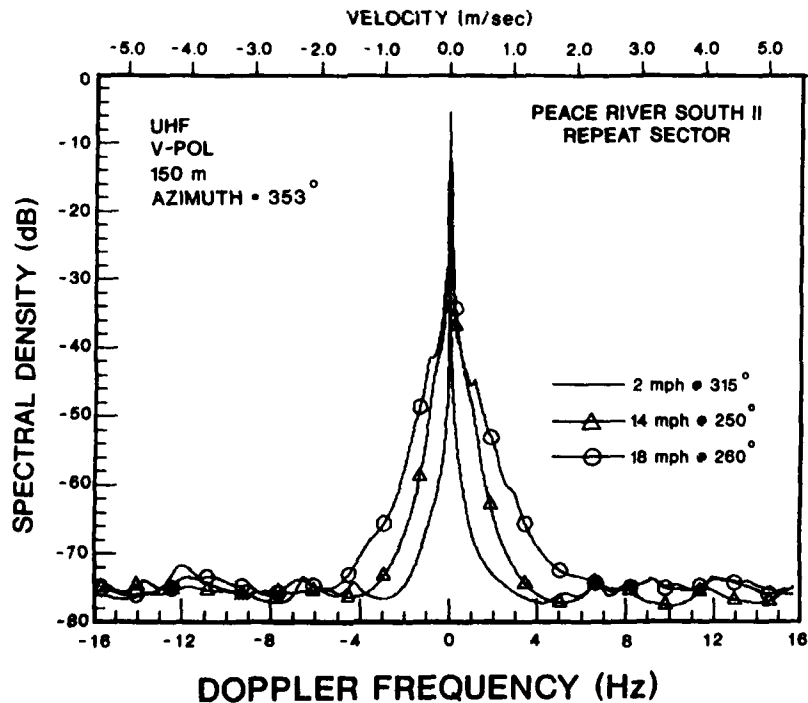


Figure 18. Average NE spectra of UHF clutter for the REPEAT sector of Peace River South II, Alberta.

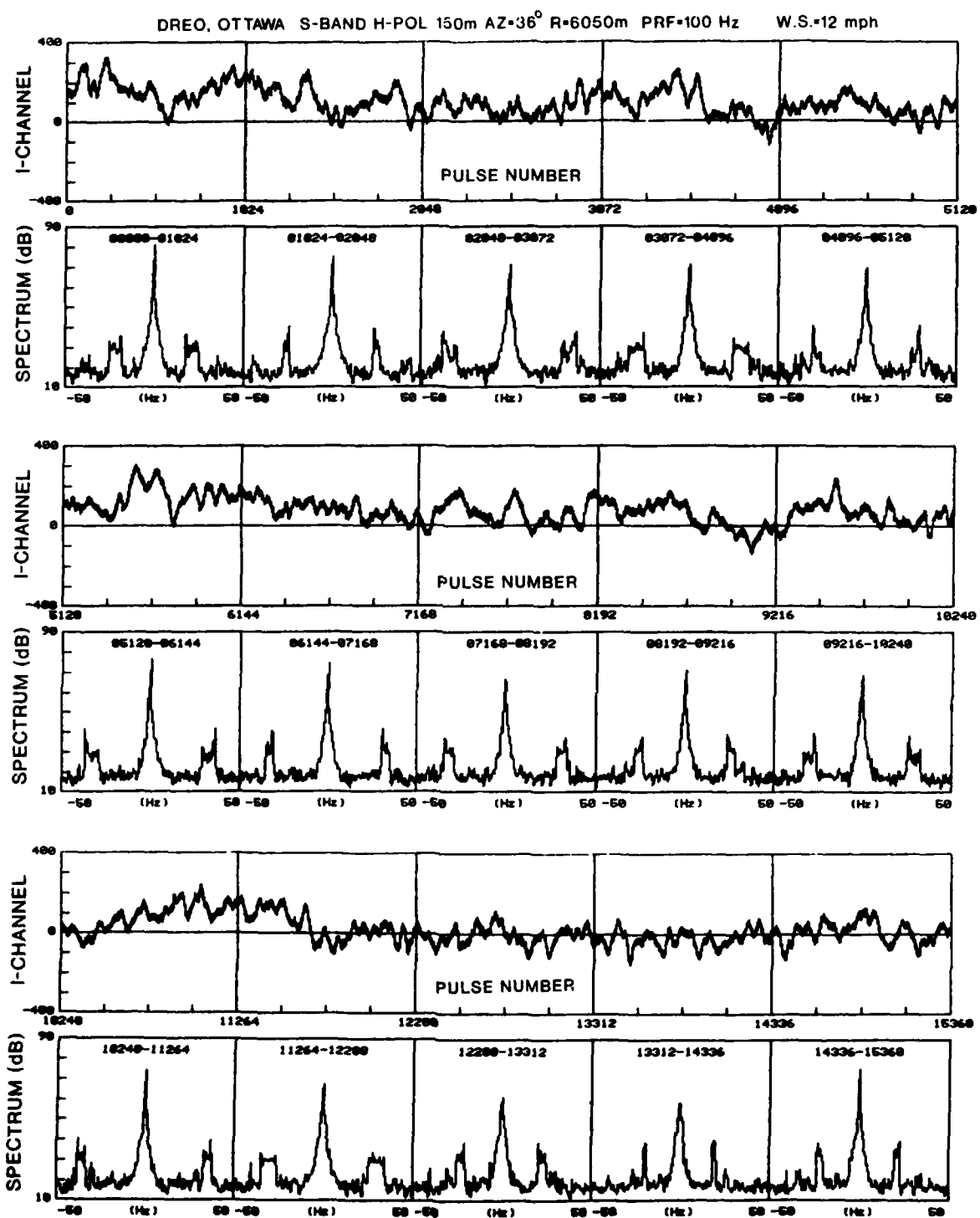


Figure 19. Sectional clutter waveform and the corresponding spectra for a DREO S-band experiment.

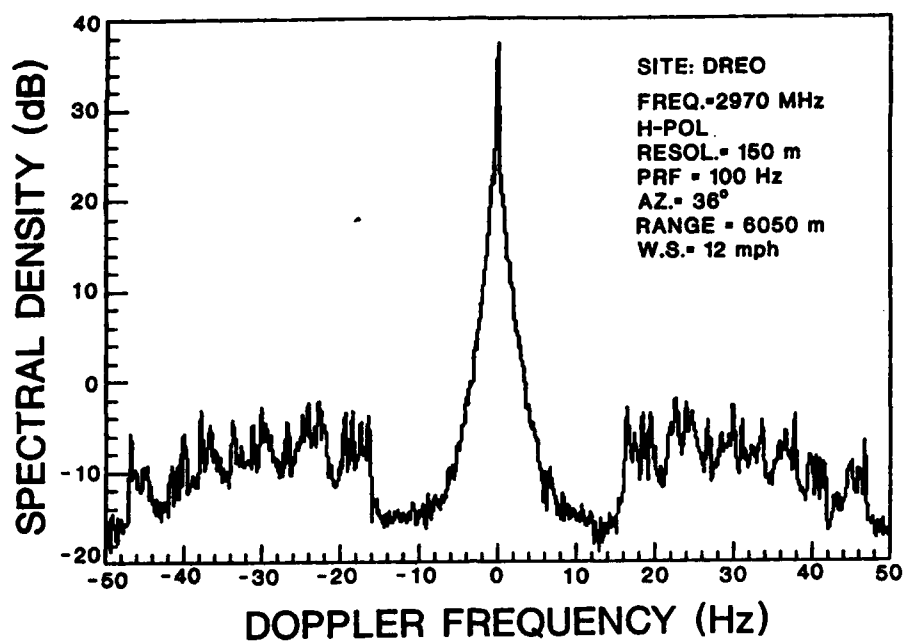


Figure 20. An S-band clutter spectrum showing the fast-diffuse component as a band-limited noise on each side of zero-Doppler

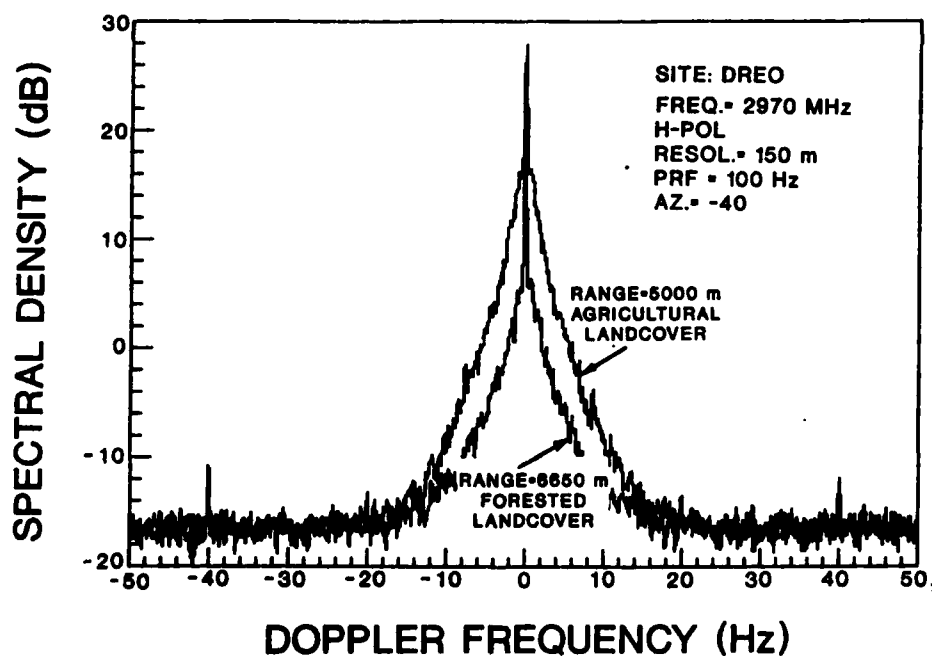


Figure 21. S-band clutter spectra of a resolution cell with forested land cover and a resolution cell with agricultural land cover at the DREO site.

In general, the coherent component may include returns from fixed objects such as large buildings and heavy but flexible objects such as large tree branches and heavy hydro wires. Returns from buildings will remain coherent even at high frequencies over a long time interval. Hence for resolution cell with pure urban (buildings) or barren land covers, the coherent component may simply be modelled as a delta function at zero-Doppler. This also applies at low frequencies (UHF and VHF) at moderate wind speeds for other land covers. Returns from heavy but flexible objects will remain coherent at very low wind speeds. However, it will become incoherent as the wind speed increases sufficiently. Thus at higher frequencies and wind speeds, the coherent component should be modelled more appropriately as a function that decreases symmetrically and exponentially on each side of zero Doppler:

$$C(f) = C'_0 \exp(-k'_c |f|) \quad (7)$$

Similarly we can model the slow-diffuse component by:

$$D^S(f) = D^{S'}_0 \exp(-k'_s |f|) \quad (8)$$

The fast-diffuse component may be modelled as band limited noise:

$$\begin{aligned} D^f(f) &= D^f_0 & |f| < f_c \\ &= 0 & |f| > f_c \end{aligned} \quad (9)$$

Since the partial spectra represented by Equations (7) and (8) dominate in different Doppler regimes, the slope of the respective spectral components can be measured separately. Expressing Eqn (7) in dB scale, we have:

$$\begin{aligned} C_{dB}(f) &= 10 \log_{10}(C'_0) - \{10 \log_{10}(e)\} k'_c |f| \\ &= C_0 - k_c |f| \end{aligned} \quad (10)$$

where k_c is in dB/Hz, and e is the base of natural logarithm.

Similarly

$$\begin{aligned} D^S_{dB}(f) &= 10 \log_{10}(D^{S'}_0) - \{10 \log_{10}(e)\} k'_s |f| \\ &= D^S_0 - k_s |f| \end{aligned} \quad (11)$$

Figure 22 depicts the symbolic diagram of the composite ground-clutter spectral model. The pertinent model parameters are k_c , k_s (the spectral slopes of the coherent and slow-diffuse components, respectively), C_0 , D^S_0 , D^f_0 (the spectral densities of the coherent, slow-diffuse and the fast-diffuse components at zero Doppler), and f_c (the cutoff frequency of the fast-diffuse component). In Section 3.3 we shall present results from which information concerning these parameters may be derived.

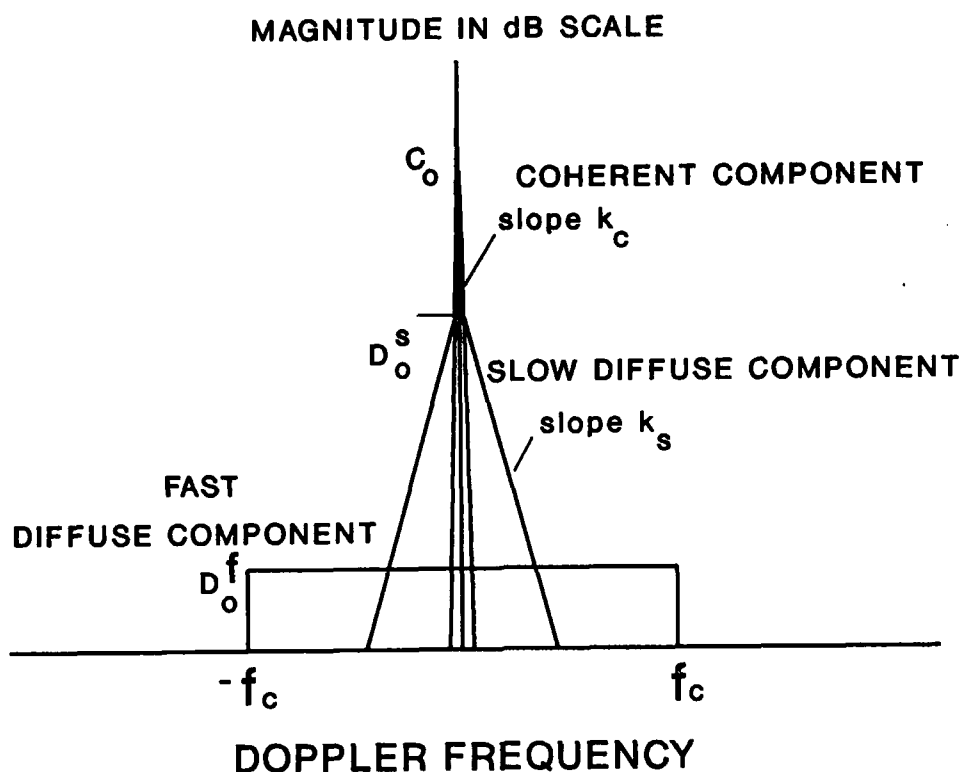


Figure 22. Symbolic diagram of the composite ground clutter model.

3.3 Model parameters and their dependence on wind speed, wind direction and land covers.

3.3.1 Spectral slopes of the coherent and the slow-diffuse components.

(a) Spectral slope of the coherent component

Parameter k_c , the spectral slope of the coherent component, is much more steep than k_s (that for the slow-diffuse component). As an example, in Figure 10, the X-band clutter spectrum for a wind speed of 22 mph had two distinct slopes. The first, around zero-Doppler, had a slope of about -20 dB/Hz. The second, corresponding to that of the slow-diffuse component, had a slope of -1.1 dB/Hz. This means that within a Hz, the spectral density of the coherent component would have decreased to a level below that of the slow-diffuse component. Since the coherent component occupies a very narrow spectral region around zero-Doppler, to measure its slope would require a very long observation time. Available Phase I data did not permit a comprehensive analysis of parameter k_c over a sufficiently wide range of wind speeds.

(b) Spectral slope of the slow-diffuse component.

Parameter k_s may be measured readily with available clutter data for various radar frequency as functions of wind speed.

The spectral slopes of the slow-diffuse component were measured from the averaged clutter spectra obtained from the REPEAT data of Magrath and Peace River South II, using the procedure outlined in Section 2.3. In Figure 23 we plotted the slope parameter of the slow-diffuse spectral component against the recorded wind speed. The slope parameters were estimated from the averaged ME spectrum of individual experiments. Data were available for wind speeds ranging from 2 mph to approximately 25 mph. For UHF at low wind speed (2 mph), the spectral behaviour of the slow-diffuse component deviated from the symmetrical negative exponential model. Figure 24 shows the ME spectrum of a UHF experiment (Site=Peace River South II, Frequency=465 MHz, H-Pol, Az=353°, Range=12 km). The spectrum was computed by first coherently integrating the clutter time series over 32 samples and then fitting the resulting time series with a 32-order AR model. It can be seen that the diffuse component was dominated by four distinct spectral peaks located on both sides of zero Doppler. However the diffuse component is several orders of magnitude lower than the coherent component. For VHF data, the slow-diffuse component was much smaller than the coherent component, making the estimate of the slope parameter inaccurate.

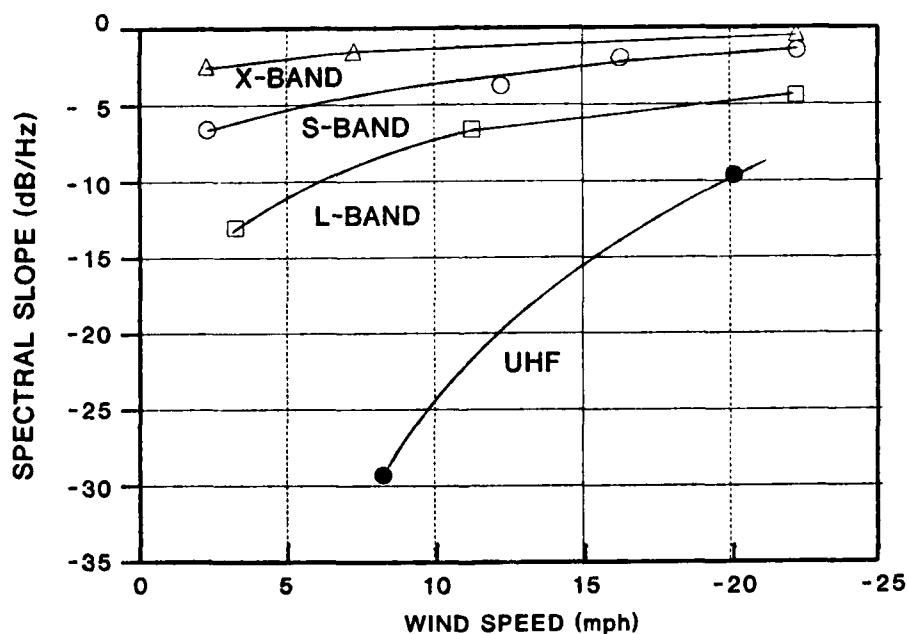


Figure 23. Slope parameter of the slow-diffuse clutter component as a function of recorded wind speed.

One can of course normalize the clutter spectra with respect to the Doppler frequency so that k_s for various radar frequencies can be plotted as a function of velocity in m/sec. From the radar signal processing perspective, greater improvement can be realized if the clutter spectrum occupies a smaller fraction of the signal bandwidth (PRF). We elect to present the results in terms of Doppler because they can easily be compared in terms of percentage of the PRF.

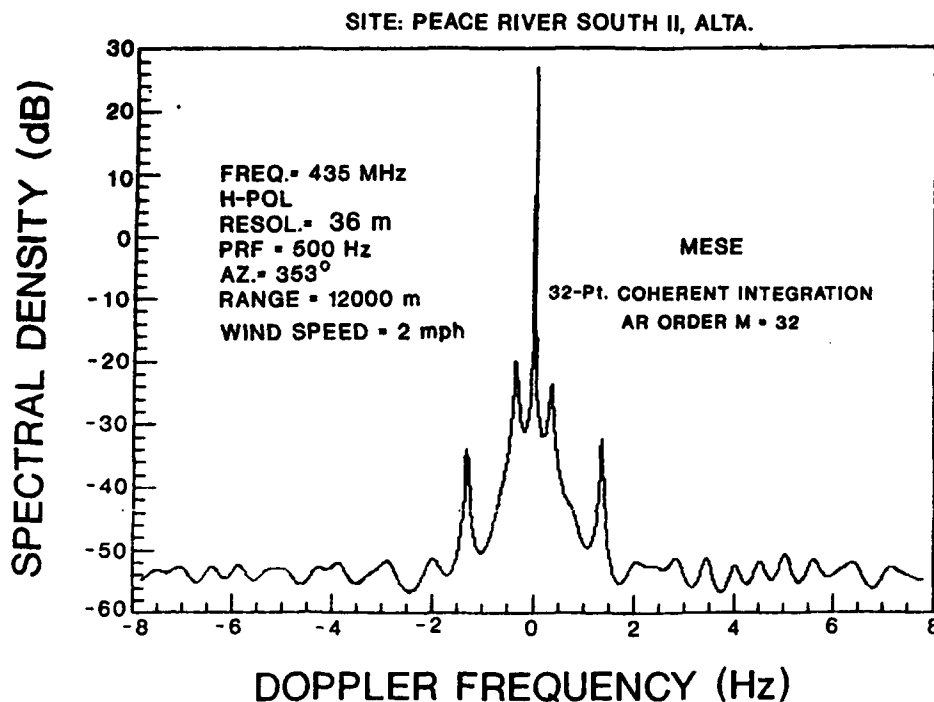
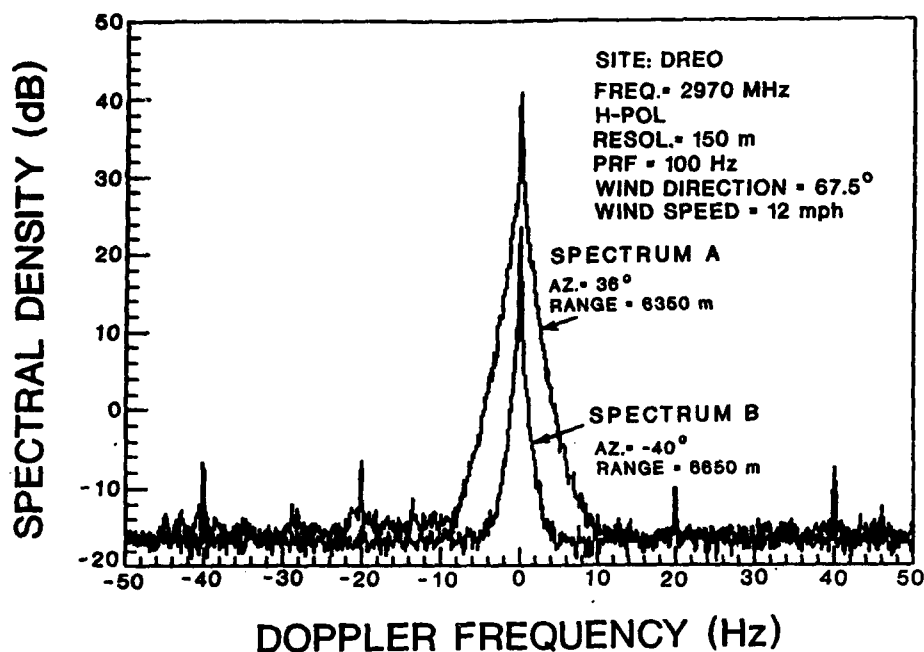


Figure 24. ME spectrum of a UHF experiment at Peace River South II, Alberta.

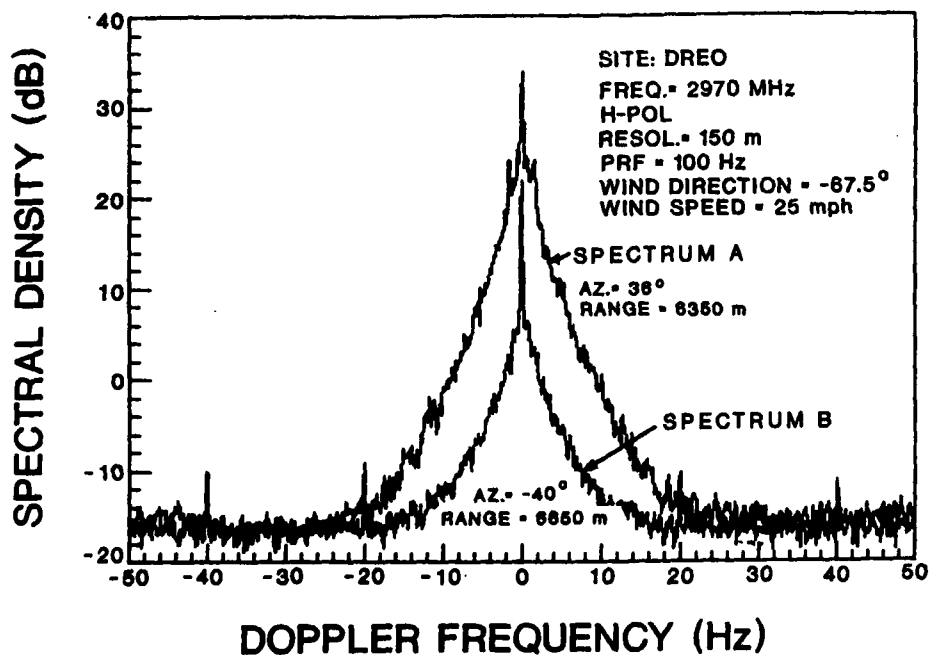
(c) Effect of wind direction.

Since the movement of most vegetations is wind-induced, we expected the spectral slope of the slow-diffuse component to be less steep (more diffuse) in the upwind direction than that in the crosswind direction. This was observed to be the case for moderate wind speeds. In Figure 25a we compared the spectra of the clutter in two resolution cells. Spectrum A was for the resolution cell located at $Az = 36^\circ$ and range = 6350m. Spectrum B was for the resolution cell located at $Az = -40^\circ$ and range = 6650m. The approximate wind speed was 12 mph from the direction of ENE (67.5°). This means that the resolution cell in the $Az = 36^\circ$ direction was near upwind, and the resolution cell in the $Az = -40^\circ$ direction was near crosswind. The slopes of the slow-diffuse component in spectrum A (upwind) and B (crosswind) were estimated to be -6 dB/Hz and -14 dB/Hz, respectively.

The difference in the spectral slopes between the upwind and crosswind cases was less noticeable at higher wind speeds. In Figure 25b we compared the spectra of the clutter in the same two resolution cells on a windy day. The approximate wind speed was 25 mph from the direction of WNW (-67.5°). Thus the resolution cell in the -40° direction was close to upwind, and the resolution cell in the $+36^\circ$ direction was close to crosswind. In this case, the slopes of spectrum A (crosswind) and spectrum B (upwind) were estimated to be -2.5 dB/Hz and -2.14 dB/Hz, respectively. This result suggested that change in the slope of the slow-diffuse component will level off at high wind speeds (typically at 20 to 25 mph).



(a) Moderate wind speed case.



(b) High wind speed case.

Figure 25. Comparison of typical clutter spectra of a resolution cell in (i) upwind and (ii) cross-wind conditions.

3.3.2 Clutter coherence factor

Parameters C_0 , D_0^s and D_0^f cannot be easily determined since they are not independent of one another. There exists a complex interrelationship among these parameters which depends on wind speed, land cover, and the relative proportions of various land covers within a resolution cell (e.g., buildings, crops, and trees). It is more practical to construct a statistical profile from which useful information concerning these parameters may be deduced.

We defined a quantity called "coherence factor" of a resolution cell as the ratio between the coherent component and the total clutter power from that cell computed over the coherence interval. We express the coherence factor in percentages:

$$CF = \frac{\left[\frac{1}{N} \sum_{n=0}^{N-1} x_n \right]^2}{\frac{1}{N} \sum_{n=0}^{N-1} |x_n|^2} \times 100 \% \quad (12)$$

Where x_n , $n=0,1,2,\dots,N-1$, are the complex clutter samples.

The coherence interval is determined by the number of pulses N and the system PRI ($N \times \text{PRI}$). The value of N should be such that the coherence interval is much longer than the time interval between revisits which is in the order of seconds. The reason is that, in order to take advantage of its coherent properties, the clutter should remain stable over a reasonably long period of time. If one is certain that the clutter will remain coherent by the time the radar revisits the same resolution cell, the coherent component can be subtracted from each subsequent return, thereby removing a substantial amount of clutter without affecting low-Doppler target signals.

The total clutter power includes both the coherent, the slow- and fast-diffuse components as well as the receiver-noise component. The fast-diffuse component is generally at least two orders of magnitude lower than the slow-diffuse component and may not even be observable at radar frequencies below L-band. Hence for a resolution cell with high clutter-to-noise ratio, the CF gives an approximate ratio of the coherent component to the sum of the coherent component and the slow-diffuse component. By examining the distribution of the CF for various land covers and wind speeds, it is possible to derive the relative magnitudes of C_0 and D_0^s statistically for resolution cells with similar land covers.

Figure 26 compares the distributions of the coherence factor of S-band clutter at the DREO site for three different wind speeds. There were 1200 resolution cells within the sector where data were collected. Approximately half of these resolution cells were located on the Ottawa River. These were excluded from the analysis since clutter from these cells represent mostly reflection from water. The remaining resolution cells were classified into three categories: (i) urban, (ii) agricultural and (iii) forested.

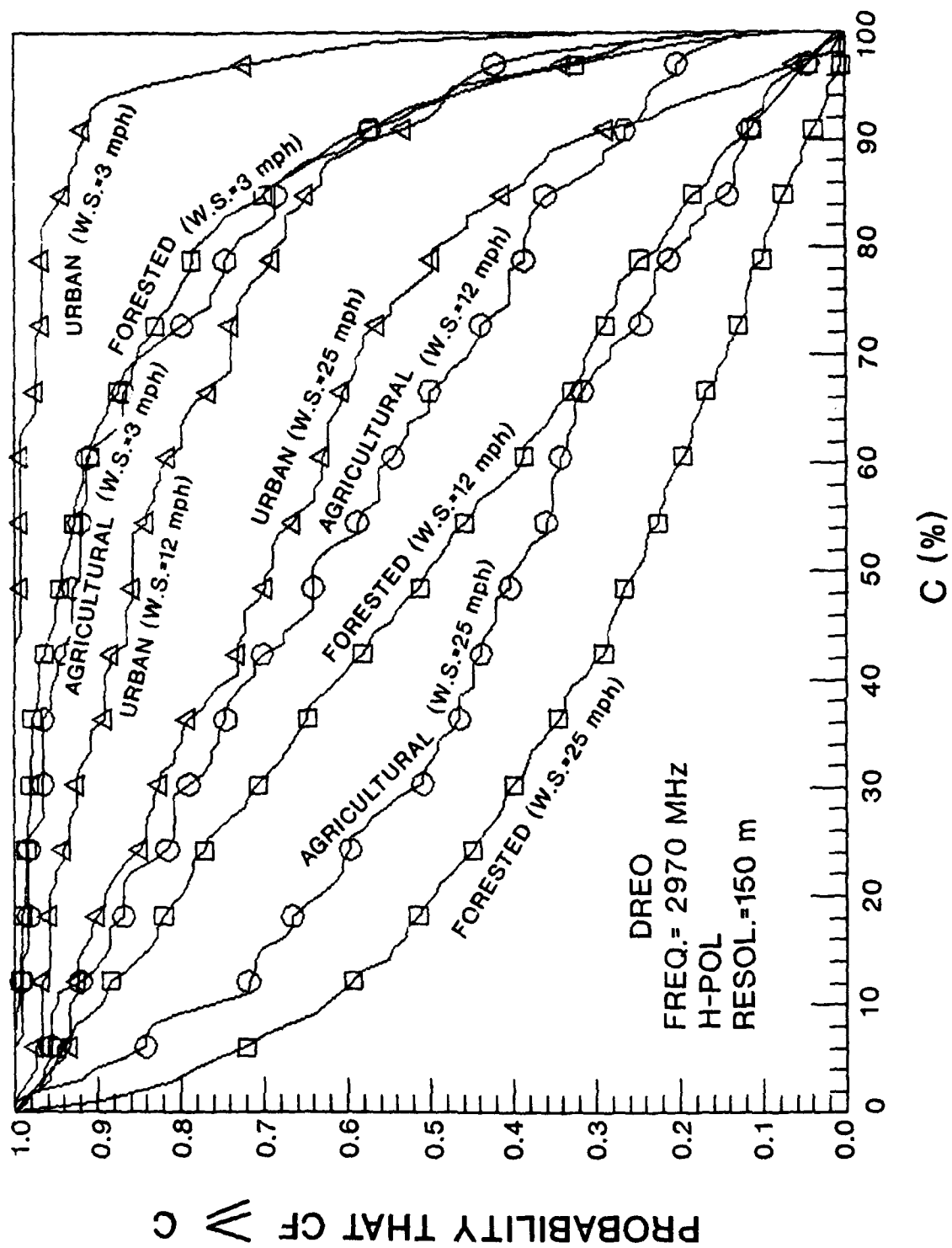


Figure 26. Comparison of the distributions of the coherence factor for S-band clutter at the DREO site in different wind-speed conditions.

Classification was performed through interpretation of high resolution aerial photographs of the DREO site. The urban land cover included residential and commercial buildings, highways, parking lots, terrain ridges and shore lines. The agricultural land cover included mostly fields with no trees visible from the aerial photos but could include some farm buildings. The forested land cover included areas covered with trees. There were 108, 109 and 387 resolution cells classified as having urban, agricultural and forested land covers respectively.

The coherence factor of the clutter from each resolution cell was computed ($N = 30720$ pulses and $PRI = 10$ msec). The number of cells whose coherence factor exceeded a given percentage was counted. The number of occurrences divided by the total sample size gave approximately the probability of finding a resolution cell with a CF greater than or equal to a specific CF value.

At low wind speeds (3 mph), the probability of finding an urban resolution cell with a coherence factor greater than or equal to 90% was over 0.9. At moderate to high (10 – 25 mph) wind speeds, this probability reduced to about 0.55, still very high. In addition, the probability of finding an urban cell with a CF of more than 50 % remained high (over 0.7) even at high wind speeds.

For agricultural areas, the probability of finding a resolution cell with a CF of at least 90% was about 0.55 at low wind speed (3 mph). However it reduced to values of 0.3 and 0.1 as the wind speed increased to 12 and 25 mph, respectively.

For forested areas, the number of resolution cells with a CF value of at least 90% was comparable to the agricultural case (0.55) at low wind speeds. As the wind speed increased to over 12 mph, the probability reduced to 0.1. At high wind speeds, the clutter from most forested cells was essentially incoherent.

As discussed in Section 2.1, the REPEAT data offered clutter data with sufficiently wide range of wind speeds at various radar frequencies. To gain some insight into the behaviour of clutter coherence factor at other frequencies for various land covers and wind speeds, we analyzed data from the REPEAT sectors of the Magrath and Peace River South II sites. Detailed high resolution aerial photographs of the two sites showed that the REPEAT sector in Magrath comprised resolution cells with either agricultural or rangeland land cover. For the Peace River South II site, the resolution cells in the REPEAT sector were classified either as deciduous forested or agricultural land.

Theoretically, the coherence factor may be obtained by first computing the FFT of the time series and then taking the ratio between the squared magnitude of the first term and the sum of the squared magnitude of all frequency indices. The FFT is defined as:

$$F_k = \frac{1}{N} \sum_{n=0}^{N-1} x_n \exp(-j2\pi nk/N) \quad (13)$$

where $x_n, n=0,1,2,\dots,N-1$, represent the complex clutter time series from a resolution cell.

If we set the frequency index k of Eqn(13) to zero, F_0^2 will be identical to the numerator of Eqn(12) which is the coherent component. The sum of the squared magnitudes of all frequency indices F_k , $k=0,1,2,\dots,N-1$, is equal to the denominator of Eqn(12) by virtue of Parseval's theorem. However, the dwell employed by the REPEAT data was short (typically 1024 pulses). The PRF's employed for X-, S-, L-band and UHF experiments were 2kHz, 3kHz, 2kHz and 1kHz, corresponding to observation times of 0.5, 0.3333, 0.5 and 1 second, respectively. This means that the CF computed by directly processing the clutter time series using a 1024-point FFT only measures clutter coherence over a period of less than a second. Since we are interested in knowing the clutter coherence factor over a much longer time interval, the FFT method is unsuitable.

The deficiency of the FFT method may be overcome by replacing the FFT-spectrum in Eqn(13) by the ME spectrum of Eqn(4). The procedures for obtaining these results are as follows. The 1024-point time series for each resolution cell within the repeat sectors were first coherently integrated and its ME spectrum computed. The values of the zero-Doppler component and the total clutter power were obtained from the ME-spectrum and substituted into Eqn (12) to compute the CF. The coherent integration length and the AR model employed for each frequency are tabulated in Table III.

Table III Coherent integration length and AR model order for clutter spectrum calculation

Frequency band	Coherent integration length (no. of pulses)	AR model order	Original PRF (Hz)	Resulting Bandwidth (Hz)
X-band	16	16	2000	125.0
S-band	16	16	3000	187.5
L-band	16	16	2000	125.0
UHF	32	8	1000	31.25

Figures 27 and 28 show the distributions of the clutter coherence factor for Magrath and Peace River South II, respectively, using the procedure outlined above. It can be seen that for a fixed radar frequency, the probability of finding a resolution cell with high coherence factor decreases as the wind speed increases. For an agricultural site (Magrath) at low wind speeds, there is a large portion of resolution cells with a CF greater than 90% at most frequencies except X-band. This is probably due to the fact that returns from crops were much weaker compared with returns from fixed objects such as farm houses, and roads. For a forested site (Peace River South II), there was a much higher proportion of resolution cells with a CF less than 10 %. This means that the clutter in a forested site at frequency above L-band is essentially incoherent. For UHF there was a large proportion of resolution cells whose clutter will remain highly coherent at low to moderate wind speeds.

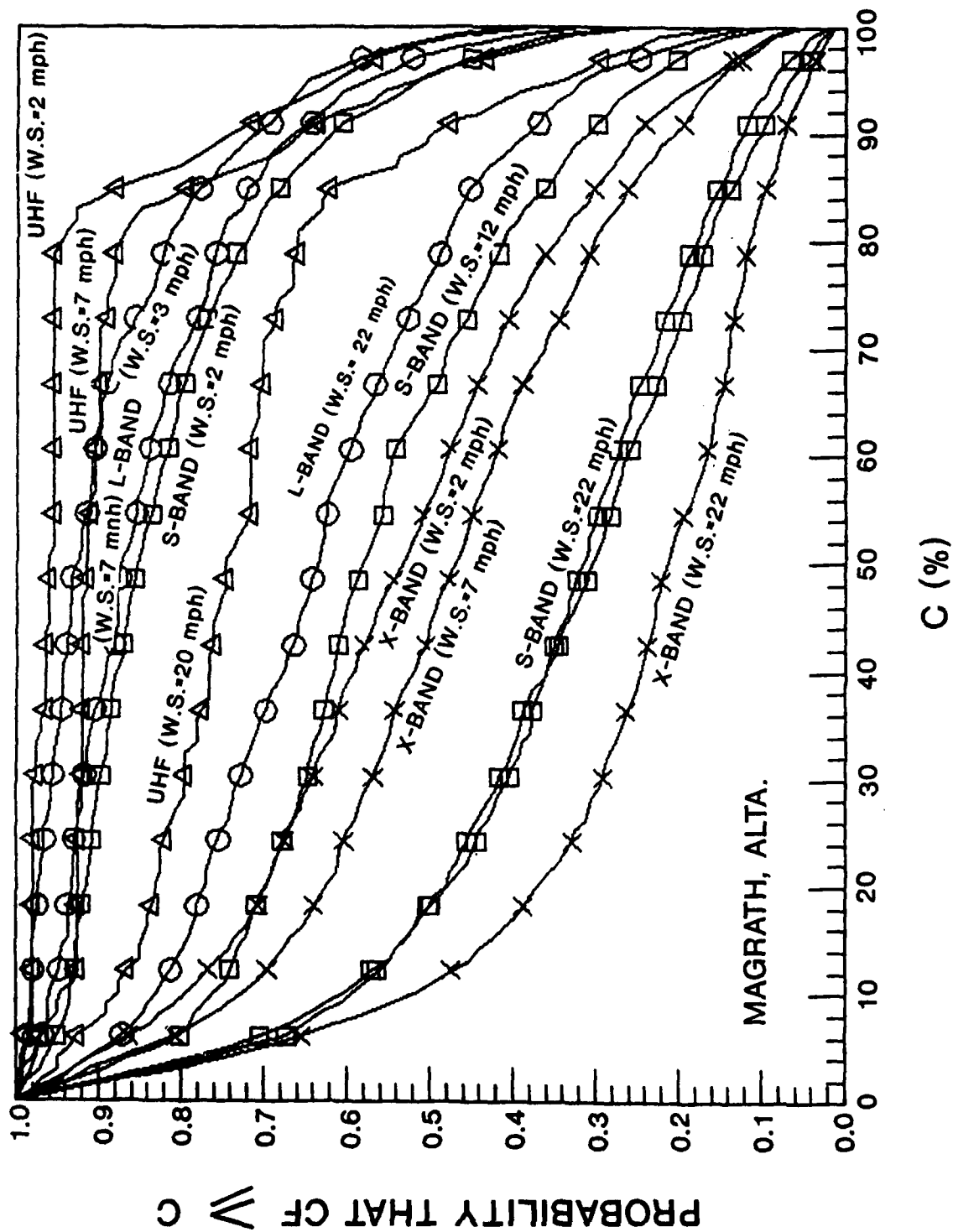


Figure 27. Distributions of the coherence factor for clutter in the REPEAT sector of Magrath, Alberta.

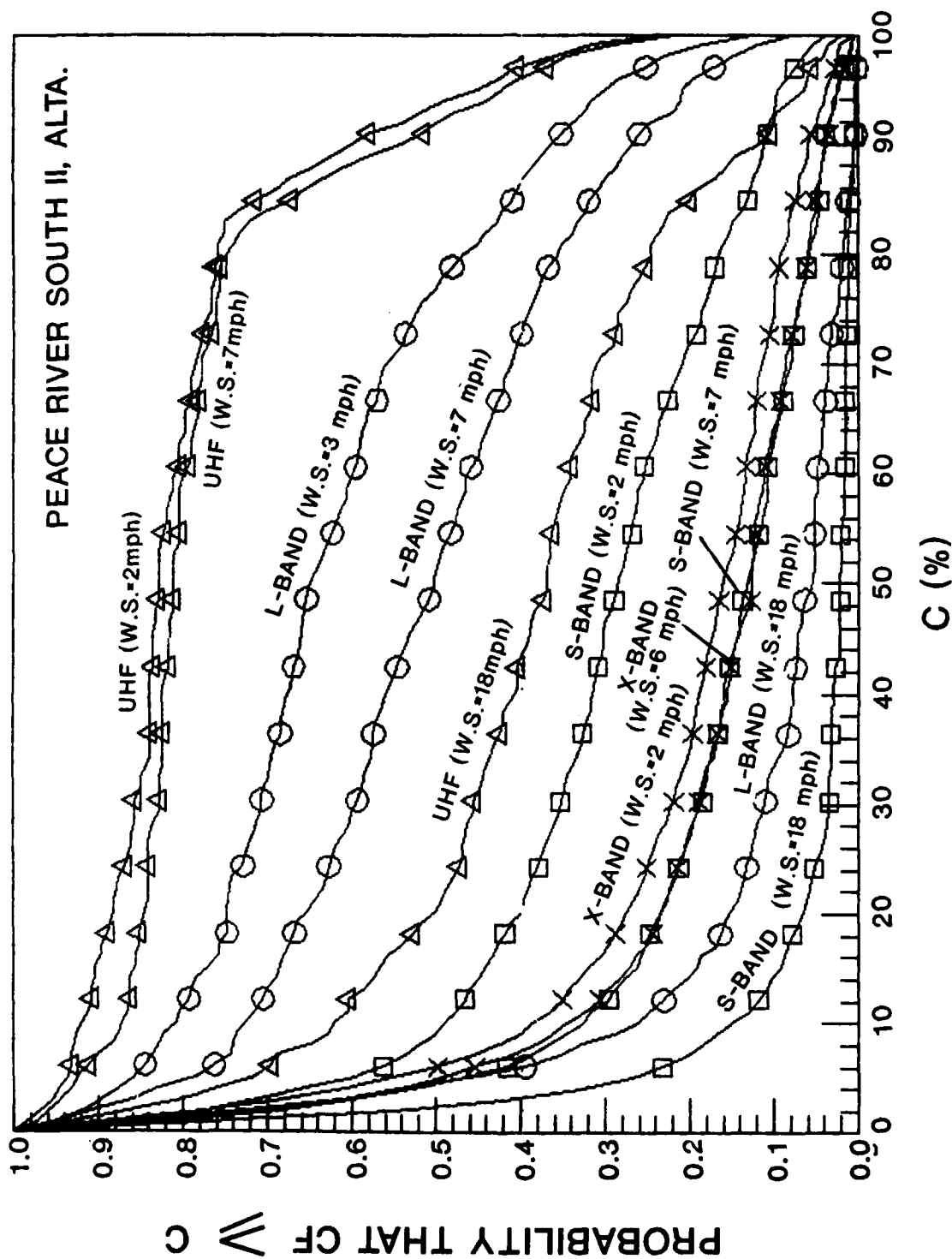


Figure 28. Distributions of the coherence factor for clutter in the REPEAT sector of Peace River South II, Alberta.

Comparing the S-band results of Figures 27 and 28 with the DREO S-band result (Figure 26) we noticed that there was a much larger proportion of resolution cells with low CF values at the Magrath and Peace River South II sites than at the DREO sites for similar wind speeds. It was conjectured that the seasons in which the data were taken could have some effect on the observed difference of the CF's. The data for Magrath were recorded in May, and the data for Peace River South II were recorded in mid October. Thus there should have been a substantial amount of vegetation and tree leaves. On the other hand, the DREO data were recorded in February, and the trees in the area were almost entirely stripped of leaves. Thus for the same wind velocity, the resulting motion of the trees at the DREO site would be less since the effective area was reduced. More analysis is required to verify this conjecture.

The results presented in this section can be used to obtain information on parameters C_0 and D_0^s statistically. For example, given a total clutter power from a resolution cell and the coherence factor, the clutter can be divided into the coherent and slow-diffuse components (assuming negligible fast-diffuse component and receiver noise). With the knowledge of k_c and k_s (Section 3.3.1), C_0 and D_0^s can be determined from Eqn(7) and Eqn(8), respectively.

3.3.3 The fast-diffuse component.

As discussed in Section 3.1, the fast-diffuse component is spatially inhomogeneous and is transient in nature. Available data did not permit meaningful quantitative results on parameters D_0^f and f_c to be derived. Fortunately, the magnitude of this component is relatively small compared with the coherent and slow-diffuse components. Its effect on radar signal processing will not become significant until both the coherent component and the slow-diffuse component have been removed. Nevertheless, the existence and spectral extent of the fast-diffuse component should be taken into consideration for MTI filter applications requiring an ultra-high improvement factor.

4. Conclusions.

4.1 Summary of results

We have carried out a detailed analysis on the spectral characteristics of low-angle ground clutter observed with coherent ground based radars. The major conclusions of this study were:

(i) The clutter spectrum as observed from a ground-based radar comprised a coherent component, a slow-diffuse component and a fast-diffuse component. The coherent component is the result of radar returns from immovable objects such as buildings, highways, mountains, and those from movable objects (tree branches, etc) at rest. The slow-diffuse component was likely the consequence of returns from movable objects such as vegetation, tree branches set in motion by the wind. This component had a moderate Doppler spread (up to several tens of Hz at X-band). The fast-diffuse component occupies a broader Doppler region than the slow-diffuse component, and its spectrum is similar to that of a band-limited noise.

(ii) The spectral shape of both the coherent component and the slow-diffuse components may be modelled by a function that decreases symmetrically and exponentially on each side of zero-Doppler frequency, except for UHF and VHF at low wind speeds. The rate of decay for the coherent component is much more rapid than that of the slow-diffuse component. It was conjectured that the symmetrical shape of these spectral components is due to the limited freedom of travel of most movable objects (vegetation, tree branches and leaves) which contribute to ground clutter. Once these objects were set in motion by wind, they behaved like pendulums. Since there are numerous objects in a resolution cell, the distribution of objects travelling towards and away from the radar is equally likely.

(iii) The fast-diffuse component was transient in nature and was most likely caused by movement of light objects (such as tree leaves) in sudden wind gusts. The magnitude of this component is usually small compared to the coherent component and the slow-diffuse component. Crops in light breezes were also observed to produce fast-diffuse components with a Doppler shift compatible with that of the prevailing wind speed.

(iv) Part of the diffuse component power could be transferred to the coherent component as the wind speed decreases.

(v) The coherence factor of ground clutter increases with decreasing radar frequency. At VHF, the coherence factor remains high for all land covers and wind speeds.

(vi) The distribution of coherence factor was site-dependent. Generally, we found more resolution cells with a high coherence factor in urban areas where the clutter results mainly from buildings. In forested areas, we found more resolution cells with a high coherence factor at low wind speeds and more cells with a low coherence factor at moderate to high wind speeds. At frequencies above L-band, the ground clutter from resolution cells with primarily forested land cover is incoherent even at very low wind speed.

(vii) Polarization has no apparent effect on observed clutter spectra. One minor exception was that weak spectral peaks were observed with X-band, V-Pol signal from agricultural areas of Magrath, Alberta at low wind speeds. These spectral peaks were likely the result of regular oscillatory motion of vegetation in light breeze. This component was absent from the X-band, H-Pol spectrum. This, however, could be because the magnitude of the fast-diffuse component was lower at horizontal polarization and consequently below noise level.

(viii) Wind direction had a direct effect on the spectral slope of the slow-diffuse component at low to moderate wind speeds (< 15 mph). The spectral slope of the slow-diffuse component was less steep in the up- and down-wind directions than in the cross-wind direction. At higher wind speeds (> 20 mph), the difference in the slopes of the slow-diffuse component in upwind and downwind cases was within the range of values observed from resolution cells in the same direction. Wind direction had a greater effect on the fast-diffuse component. For up-wind and downwind directions, the presence of a fast-diffuse component is more evident.

(ix) Clutter spectra observed from various waveform resolutions ranging from 15 m to 150 m did not show significant differences.

The spectral characteristics of ground-clutter suggested that ground clutter presents a bigger problem for slow-target detection at higher frequencies (X-, and S-bands) than at low frequencies (L-band, UHF and VHF). In Section 4.2 we shall discuss several approaches for low-speed target detection improvement which take advantage of the ground clutter spectral characteristics.

4.2 Signal Processing Improvements for Ground-based Surveillance Radars.

The findings of this study provided insights into the spectral behaviour of ground clutter in two important aspects: (i) the spectral shape of the various components and (ii) the coherence factor. These insights can be used to develop techniques to improve the performance of ground-based surveillance radars. Current state-of-the-art surveillance radars employing moving target detectors (MTD) [11] provide nearly optimum detection performance for targets whose Doppler shift is well separated from the ground clutter. Significant improvement is still possible in the detection of targets with near-zero radial velocity.

For ground-based military surveillance radars, the detection of low-flying cruise missiles in a tangential trajectory is difficult. The same can be said for civil air-traffic control radars for detection of small, slow-moving aircraft. In the following we discuss three possible approaches which could improve performance for near-zero velocity target detection of surveillance radars.

(a) Adaptive ground clutter filter.

The coherent component and the slow-diffuse component contain most of the clutter power. The spectral characteristics of these two components are predictable. For example, we found that the spectral shape of both the coherent component and the slow-diffuse component may be modelled by a function that decreases symmetrically and exponentially on each side of zero-Doppler frequency. The slope parameter of the models is a function of wind speed and radar frequency. This is a priori information which can be extracted from the clutter data.

In conventional MTD processor designs, a bank of fixed band-pass filters is used to suppress the ground clutter. The filter whose passband is occupied by the clutter spectrum is called the zero-velocity filter (ZVF). The ZVF essentially passes the clutter power with very little attenuation. This means that the target signal must be substantially greater than the clutter even though the Doppler is separated from the ground-clutter spectrum but still within the passband of the ZVF. Detection of potential targets with low or near-zero radial velocity is assisted by the so-called non-coherent clutter map. The non-coherent clutter map does not discriminate clutters with different relative spectral widths. Consequently, spectral information of the clutter is not utilized.

With good modelling information of the ground clutter spectral characteristics as a function of wind conditions, it is possible to adaptively change the coefficients of the clutter filter bank so as to optimize the bandwidth of the ZVF and the target-to-noise ratio for each filter according to the prevailing wind condition. This concept, however, is likely to have only limited benefits for radar systems employing a mechanically rotating antenna. The clutter spectrum as observed from a rotating antenna is dominated by the antenna scanning modulation. With a phased array antenna, however, a greater improvement in detection performance may be possible, particularly at higher radar frequencies (X- and S-bands).

(b) Coherent clutter maps.

The coherent clutter map [3] is the simplest way to utilize a priori spectral information of ground clutter to improve detection performance in resolution cells with a high coherence factor. A coherent-clutter map is a signal processing scheme whereby a long-term coherent average of the clutter in each resolution cell is kept in the memory of the signal processor. The coherent-clutter average from a resolution cell is subtracted from the instantaneous returns. The result is then passed onto the subsequent signal processing chain such as a Doppler processor and CFAR. A resolution cell with a high coherence factor implies that the clutter in that particular cell is stable both in amplitude and phase. This permits the coherent cancellation of large ground clutter returns without affecting the target signal even for targets with zero radial velocity. We have observed that the coherence factor for urban areas is high for most radar frequencies. Since the clutter coefficient for resolution cells with predominantly urban land cover (buildings) is usually much higher than those of other land covers, the cancellation of the coherent component of the clutter from these resolution cells will substantially improve detection performance for applications such as civil airport surveillance.

Most ground clutter suppression schemes operate on a multi-pulse basis either as pulse cancelers or as MTI filters. The effectiveness of the coherent ground clutter map depends on how much the clutter amplitude and phase differ from the stored coherent map values for a particular resolution cell. The map value can be updated periodically to accommodate long-term variation in the amplitude and phase. Thus the performance of coherent ground-clutter map also depends on how fast the clutter decorrelates (both amplitude and phase) between times of revisit. For most surveillance radars, the time between revisit is in the order of a few seconds. From what has been observed from our clutter data, the coherent clutter map will not be effective for X- and S-bands for land covers other than pure urban areas.

At lower frequencies, the coherent clutter map concept becomes practical even for land covers other than pure urban areas. In this study, we observed that the coherence factor of UHF and VHF ground clutter remained high even at high wind speeds.

As in the adaptive clutter filter concept, the coherent-clutter map should be implemented with a non-mechanically scanned antenna such as a phased array. However, it is possible to implement a coherent-clutter map in a radar system with mechanically-scanned antenna. In this case, the magnitude of contiguous returns of a transmitted pulse train will be modified by the scanning antenna pattern, even though the scatterers that generate the clutter are stationary. However for a fixed range and azimuth, this variation may be considered deterministic and can be modelled by an autocorrelation function.

In a radar system employing a mechanically-scanning antenna, the transmission of the pulse train is continuous. This means that there is no unique beginning or ending of a dwell for a given azimuth. We can, however, divide the circumference into a number of azimuthal sectors. By choosing the antenna scan rate and the radar PRF appropriately so that a pulse is transmitted exactly each time an azimuthal sector is revisited by the radar beam, the radar returns may be organized into subsequences representing the returns from each resolution cell. A coherent clutter map value is kept for the first return from each resolution cell together with the corresponding autocorrelation coefficients of the clutter time series. The coherent clutter estimates for the remaining pulses are computed from the stored map value and the autocorrelation function of that cell.

(c) Predictive Coherent Clutter Map.

An extension of the coherent clutter map concept is the predictive coherent clutter map. That is, we analyze ground-clutter spectra for various land covers and wind conditions. Predictive models are then derived and catalogued from the observed clutter spectral characteristics. The model will be used to estimate the ground-clutter amplitude and phase from each resolution cell for the next revisit time, based on past observed samples. The estimate would be subtracted coherently from the actual return. If the estimate is accurate, the residual clutter should be significantly lower than the original clutter sample without affecting target components that may be present. A viable model is the autoregressive model. The predictive coherent-clutter map concept requires accurate modelling information.

In addition to accurate modelling information, the prediction of random process requires adequate sampling (at Nyquist rate). An electronically scanned antenna is more suitable for implementing the predictive coherent clutter map because its look direction is not constrained by the mechanical boresight of the antenna. With an electronically scanned antenna one can have a much more frequent revisit to a resolution cell, thereby obtaining a higher sampling rate of the clutter process than possible with a mechanically scanned antenna. More research is needed to determine the feasibility of the predictive clutter map approach, the achievable performance improvement and the operational requirements.

5. REFERENCES

- [1] Nathanson, F.E., "Radar Design Principles, Signal Processing, and the Environment", McGraw-Hill, New York, New York, 1969.
- [2] Dillard, G.M. and Rickard, J.T., "A Distribution-Free Doppler Processor", IEEE Trans. Aero. and Elect. Systems, Vol. AES-10, No.4, July 1974, pp.479-486.
- [3] Bird, J.S., "Coherent Processing of Ground Clutter to Improve Low-Doppler Target Detection and Identification", NATO AGARD Symposium on Target Signatures, London, U.K., October 1984, pp. 3-1 to 3-10.
- [4] Billingsley, J.B., "Phase One Master Directory File", MIT Lincoln Laboratory CMDT Project Memorandum No. 45 PM-CMT-0003, September 1985.

- [5] Billingsley, J.B. and Larrabee, J.F., "Multi-Frequency Measurement of Radar Ground Clutter at 42 Sites", Lincoln Laboratory Project Report No. CMT-87, to be published in December 1989.
- [6] Billingsley, J.B. and Larrabee, J.F., "Measured Spectral Extent of L- and X-band Radar Reflections from Wind-Blown Trees", Lincoln Laboratory Project Report No. CMT-57, February 1987.
- [7] Papoulis, A., "Maximum Entropy and Spectral Estimation: A Review", IEEE Trans. Acoust. Speech Signal Process., Vol. ASSP-29, pp.1176-1186, December 1981.
- [8] Burg, J.P., "Maximum Entropy Spectral Analysis", Ph.D Thesis, Stanford University, Stanford, CA, 1975.
- [9] Jaynes, E.T., "On the Rationale of Maximum Entropy Method", Proc. IEEE, Vol. 70, pp. 939-952, September 1982
- [10] Akaike, H., "Fitting Autoregressive Models for Prediction", Ann. Inst. Stat. Math., Vol. 21, 1969.
- [11] Karp, D. and Anderson, J.R., "Moving Target Detector (Mod II) Summary Report", Lincoln Laboratory Technical Report No. FAA-RD-80-77, November 1981.

6. ACKNOWLEDGEMENT

The author thanks the U.S. Defence Advanced Research Projects Agency and the personnel of Group 45 of the MIT Lincoln Laboratory for providing the Phase I ground clutter data used in the analysis.

SECURITY CLASSIFICATION OF FORM
(highest classification of Title, Abstract, Keywords)

DOCUMENT CONTROL DATA

(Security classification of title, body of abstract and indexing annotation must be entered when the overall document is classified)

1. ORIGINATOR (the name and address of the organization preparing the document. Organizations for whom the document was prepared, e.g. Establishment sponsoring a contractor's report, or tasking agency, are entered in section 8.) DEFENCE RESEARCH ESTABLISHMENT OTTAWA		2. SECURITY CLASSIFICATION (overall security classification of the document including special warning terms if applicable) UNCLASSIFIED	
3. TITLE (the complete document title as indicated on the title page. Its classification should be indicated by the appropriate abbreviation (S,C,R or U) in parentheses after the title.) SPECTRAL CHARACTERISTICS OF LOW-ANGLE RADAR GROUND CLUTTER			
4. AUTHORS (Last name, first name, middle initial) CHAN, HING C.			
5. DATE OF PUBLICATION (month and year of publication of document) DECEMBER, 1989		6a. NO. OF PAGES (total containing information. Include Annexes, Appendices, etc.) 52	6b. NO. OF REFS (total cited in document) 11
7. DESCRIPTIVE NOTES (the category of the document, e.g. technical report, technical note or memorandum. If appropriate, enter the type of report, e.g. interim, progress, summary, annual or final. Give the inclusive dates when a specific reporting period is covered.) TECHNICAL REPORT			
8. SPONSORING ACTIVITY (the name of the department project office or laboratory sponsoring the research and development. Include the address.) DEFENCE RESEARCH ESTABLISHMENT OTTAWA, 3701 CARLING AVENUE, OTTAWA, ONTARIO, K1A 0Z4			
9a. PROJECT OR GRANT NO. (if appropriate, the applicable research and development project or grant number under which the document was written. Please specify whether project or grant) 041LC12		9b. CONTRACT NO. (if appropriate, the applicable number under which the document was written)	
10a. ORIGINATOR'S DOCUMENT NUMBER (the official document number by which the document is identified by the originating activity. This number must be unique to this document.) DREO REPORT No. 1020		10b. OTHER DOCUMENT NOS. (Any other numbers which may be assigned this document either by the originator or by the sponsor)	
11. DOCUMENT AVAILABILITY (any limitations on further dissemination of the document, other than those imposed by security classification) <input checked="" type="checkbox"/> (X) Unlimited distribution <input type="checkbox"/> () Distribution limited to defence departments and defence contractors; further distribution only as approved <input type="checkbox"/> () Distribution limited to defence departments and Canadian defence contractors; further distribution only as approved <input type="checkbox"/> () Distribution limited to government departments and agencies; further distribution only as approved <input type="checkbox"/> () Distribution limited to defence departments; further distribution only as approved <input type="checkbox"/> () Other (please specify):			
12. DOCUMENT ANNOUNCEMENT (any limitation to the bibliographic announcement of this document. This will normally correspond to the Document Availability (11). However, where further distribution (beyond the audience specified in 11) is possible, a wider announcement audience may be selected.) UNLIMITED			

UNCLASSIFIED

SECURITY CLASSIFICATION OF FORM

13. ABSTRACT (a brief and factual summary of the document. It may also appear elsewhere in the body of the document itself. It is highly desirable that the abstract of classified documents be unclassified. Each paragraph of the abstract shall begin with an indication of the security classification of the information in the paragraph (unless the document itself is unclassified) represented as (S), (C), (R), or (U). It is not necessary to include here abstracts in both official languages unless the text is bilingual).

A detailed analysis of low-angle ground clutter spectral characteristics was carried out using the MIT Lincoln Laboratory Phase I data and the DREO S-band clutter data. Both the fast Fourier transform and a super-resolution spectral analysis technique were used. Results showed that a ground clutter spectrum comprises three components, namely, (a) a coherent component, (b) a slow-diffuse component and (c) a fast-diffuse component. Both the coherent component and the slow-diffuse component may be modelled as a symmetrical negative exponential density function. The fast-diffuse component may be modelled as a band-limited noise. Model parameters included the spectral slopes, the spectral density at zero Doppler and the cutoff frequency of the fast-diffuse component. The spectral slopes of the slow-diffuse component at various wind speeds have been calculated from the clutter data. The spectral densities of the various components were inter-related through wind speed and land cover. These parameters can be determined statistically from the clutter coherence factor for various land covers and wind speeds. The results of this analysis provided additional insights into ground clutter and can be used to develop signal processing techniques for improved low-velocity target detection in clutter-limited environments.

14. KEYWORDS, DESCRIPTORS or IDENTIFIERS (technically meaningful terms or short phrases that characterize a document and could be helpful in cataloguing the document. They should be selected so that no security classification is required. Identifiers, such as equipment model designation, trade name, military project code name, geographic location may also be included. If possible keywords should be selected from a published thesaurus, e.g. Thesaurus of Engineering and Scientific Terms (TEST) and that thesaurus-identified. If it is not possible to select indexing terms which are Unclassified, the classification of each should be indicated as with the title.)

RADAR, GROUND CLUTTER, SPECTRUM, CLUTTER MODEL

UNCLASSIFIED

SECURITY CLASSIFICATION OF FORM